Microfacies of middle Devonian transgressive carbonates of central midcontinent, USA : shallowing-upward sequences in a deepening-upward eustatic trend

Autor(en): **Kocken, Roger J. / Carozzi, Albert V.**

Objekttyp: **Article**

Zeitschrift: **Archives des sciences et compte rendu des séances de la Société**

Band (Jahr): **44 (1991)**

Heft 3: **Archives des Sciences**

PDF erstellt am: **23.07.2024**

Persistenter Link: https://doi.org/10.5169/seals-740209

Archs Sci. Genève	Vol. 44	Fasc. 3	pp. 371-415	Décembre 1991

MICROFACIES OF MIDDLE DEVONIAN TRANSGRESSIVE CARBONATES OF CENTRAL MIDCONTINENT, U. S. A.: SHALLOWING-UPWARD SEQUENCES IN A DEEPENING-UPWARD EUSTATIC TREND

BY

Roger J. KOCKEN and Albert V. CAROZZI[1]

ABSTRACT

Twelve normal marine and twelve hypersaline microfacies were identified petrographically in the Middle Devonian Wapsipinicon Formation, Cedar Valley Limestone, Grand Tower Limestone and Lingle Formation in Illinois, eastern Iowa and Missouri. The vertical succession and statistical analysis of microfacies permitted recognition of four ideal shallowing-upward sequences which were converted into horizontal depositional models.

Model 1 represents the normal marine Grand Tower Limestone and Lingle Formation that occur south of the Sangamon Arch. It is a carbonate ramp with a quartz sand beach. Model 2 represents the normal marine Cedar Valley Limestone north of the Sangamon Arch. It consists, in an offshore direction of an intertidal flat, ecologically zoned lagoon, stromatoporoid buildup, slope and basinal environments. Model 3 represents the basal members of the Wapsipinicon Formation. It is a partly anoxic hypersaline environment consisting of a quartz sand beach, evaporitic flat, stromatolitic ridge, and an anoxic lagoon. Model 4 is a hypersaline environment with an inner lagoon and is applicable to parts of the Wapsipinicon Formation, Geneva Dolomite and Cedar Valley Limestone. This model consists of a quartz sand beach, evaporitic flat, inner lagoon, stromatolitic ridge, and an outer lagoon.

Separate diagenetic evolutions were recognized for the normal marine and hypersaline microfacies. The normal marine microfacies display diagenetic features indicating an evolution starting with marine phreatic, and proceeding through marine vadose, meteoric vadose, undersaturated meteoric phreatic, saturated meteoric phreatic, mixed marine-meteoric and ending with burial. Diagenesis of the hypersaline microfacies is dominated by early dolomitization and formation of collapse breccias by dissolution of halite. The diagenetic sequence for the hypersaline microfacies is marine phreatic, marine vadose-evaporitic, meteoric vadose, meteoric phreatic, mixed marine-meteoric, and burial.

Thirteen shallowing-upward cycles were recognized which, in the context of local subsidence and global eustatic sea level rise of the Middle Devonian, reach their peaks in successively deeper water, forming a larger sequence with a deepening-upward trend. This situation which terminates in basinal shales indicates that subsidence and eustatic sea level rise overcame a series of unsuccessful accretionary attempts by carbonate production and accumulation. These results correlate well with published Middle Devonian sea level curves and confirm that the Middle Devonian was a time of oscillating sea level rise.

---

[1] Department of Geology, University of Illinois at Urbana-Champaign, Urbana, IL 61801-2999 (U.S.A.).

RÉSUMÉ

Douze microfaciès marins et douze microfaciès hypersalins ont été identifiés pétrographiquement dans les formations de Wapsipinicon, Cedar Valley Limestone, Grand Tower Limestone et Lingle du Dévonien moyen de l'Illinois, Iowa occidental et Missouri. La succession verticale et l'analyse statistique des microfaciès a permis de reconnaître quatre séquences idéales à profondeur décroissante qui ont été converties en autant de modèles dépositionels horizontaux.

Le modèle 1 représente le Grand Tower Limestone et la Lingle Formation, milieux marins normaux développés au sud de la Sangamon Arch. Il s'agit d'une rampe carbonatée avec une plage de sable quartzeux. Le modèle 2 représente le Cedar Valley Limestone au nord de la Sangamon Arch. Il comprend en direction de la mer les milieux suivants: platier intertidal, lagune écologiquement zonée, construction récifale de stromatoporoïdes, pente, et bassin. Le modèle 3 représente les membres de la base de la Wapsipinicon Formation. Il s'agit d'un milieu en partie anoxique et hypersalin formé d'une plage de sable quartzeux, platier évaporitique, barrière stromatolitique et lagune anoxique. Le modèle 4 représente un milieu hypersalin avec une lagune interne. Il est applicable à une partie de la Wapsipinicon Formation, la Geneva Dolomite et le Cedar Valley Limestone. Ce modèle comprend une plage de sable quartzeux, un platier évaporitique, une lagune interne, une barre stromatolitique et une lagune externe.

Les microfaciès marins et hypersalins ont subi des évolutions diagénétiques distinctes. Les microfaciès marins normaux montrent une évolution qui débute par le milieu marin phréatique et se poursuit par marin vadose, eau douce vadose, eau douce phréatique sous-saturée, eau douce phréatique saturée, mixte marin-eau douce, et se termine par l'enfouissement. La diagenèse des faciès hypersalins est dominée par une dolomitisation précoce et la formation de brèches d'effondrement par dissolution de halite. La séquence diagénétique comprend les milieux suivants: marin phréatique, marin vadose-évaporitique, eau douce vadose, eau douce phréatique, mixte marin-eau douce, et enfouissement.

Treize cycles à profondeur décroissante ont été reconnus qui, dans le contexte de la subsidence locale et de la montée eustatique globale du niveau des mers au Dévonien moyen, atteignent successivement leurs sommets en profondeur d'eau croissante formant ainsi une longue séquence de tendance à l'approfondissement. Cette situation qui se termine par des shales basinaux indique que la subsidence et la montée eustatique du niveau des mers ont surmonté une série d'essais infructueux de la production et de l'accumulation des carbonates. Ces résultats sont en excellente corrélation avec les courbes de variation du niveau des mers publiées pour le Dévonien moyen et confirment que cet espace de temps était une époque de montée oscillatoire du niveau des mers.

INTRODUCTION AND REGIONAL GEOLOGICAL SETTING

The Middle Devonian of eastern Iowa, Missouri and Illinois consists mainly of carbonates with lesser amounts of shale, sandstone and evaporites. The purpose of this study, based on whole rock cores and outcrops, was first to develop a regional synthesis of the depositional environments and related diagenetic evolutions, and second to establish the cyclicity of the Middle Devonian in the investigated area and relate it to local subsidence and global eustatic sea level rise.

The discontinuous distribution of outcrops in Iowa, Missouri and Illinois, different lithologies and small age differences, resulted in numerous formations and members used in this investigation (Figure 1). The evolution of the stratigraphic terminology and correlation problems were reviewed by Kocken (1989). For the purpose of this study it is sufficient to point out that during most of Middle Devonian time, Iowa, Missouri and Illinois were incompletely divided into two depocenters by the emergent Sangamon Arch, which extended from the Ozark Dome as a structure plunging NE toward central

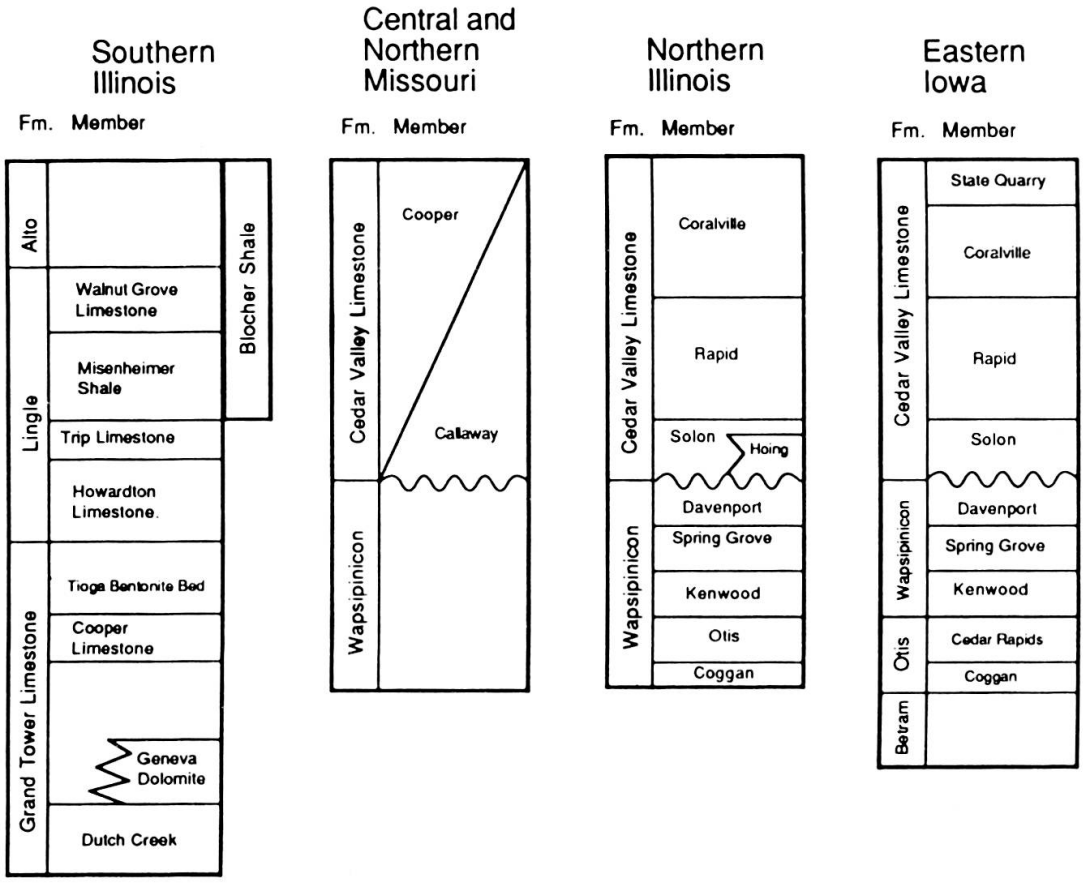

FIG. 1.

Middle Devonian correlation chart (modified from Bunker and others,1988; Collinson and others,1967; Collinson, 1988).

Illinois. In the center of the Illinois Basin, the Middle Devonian is about 120 meters thick and consists of the Grand Tower Limestone, Lingle and Alto Formations. The sequence thins to zero over the Sangamon Arch (Figure 2) and is over 150 meters thick in west-central Iowa, where it consists of the Wapsipinicon Formation and Cedar Valley Limestone.

On the basis of recent syntheses (Bunker and others,1988; Collinson and others, 1967; Collinson, 1988) the following environmental evolution occurred in the investigated area. During Early Devonian, most of Iowa, Missouri and Illinois were being actively eroded with removal of hundreds of meters of older Ordovician and Silurian formations. Only in the center of the Illinois Basin were rocks of Early Devonian age deposited. Starting in middle Early Devonian, seas started to transgress over most of the interior of North America. This transgression resulted in deposition of the Kaskaskia Sequence. The Middle Devonian occurs at its base in the study area. During the Devonian, Illinois was located at about 20° south latitude, which favored the development of carbonates and evaporites. In the Appalachian Region, the Acadian Orogeny

was taking place, however tectonic activity did not supply large amounts of clastic material to this area until Late Devonian. During most of Middle Devonian time, the Sangamon Arch, an active structural feature from Late Silurian to Early Mississippian, separated the hypersaline waters in Iowa, Missouri and Michigan from the normal marine waters to the south. This separation can be illustrated by comparing the fine-grained, evaporite-bearing, unfossiliferous Wapsipinicon Formation with the highly-fossiliferous Grand Tower Limestone and Lingle Formation. With continued transgression, the Sangamon Arch essentially disappeared during late Middle Devonian. By Late Devonian, increasing orogenic activity in the Appalachians, continued sea level rise, westward building of the Catskill Delta, and subsidence centered in Iowa and southern Illinois, combined to cover the Middle Devonian sequence with up to 100 meters of shales belonging to the New Albany Group.

Although most of the sequences in the study area show only gradual thickening toward the two depocenters, a pronounced thickening (over 120 meters of Middle Devonian) occurs in the Wittenberg Trough (Figure 2). Meents and Swann (1965) concluded that the Wittenberg Trough was a partially fault-bounded, actively subsiding structural feature from Early Devonian to Early Mississippian. It was about 110 kilometers long and 1 to 16 kilometers wide with water depths ranging from 30 meters to over 300 meters. The Wittenberg Trough was partially destroyed by uplift and erosion related to post-Mississippian fault movements.

Johnson and others (1985) constructed a detailed, qualitative eustatic sea level curve for the Devonian (Figure 3). Their curve was developed by comparing transgressive-regressive cycles in five distinct regions (mainly outer shelf areas) of varying lithology in North America and Europe. Conodonts were used to date the transgressive-regressive cycles and to demonstrate their simultaneous occurrence in the five regions. During Middle Devonian time, the overall trend was for rising sea level. Johnson and others (1985) recognized five transgressive-regressive cycles in Middle Devonian time labeled Ic to IIb (Figure 3). The most important feature is the fall in sea level at the top of cycle If which relates to the unconformity between the Wapsipinicon Formation and Cedar Valley Limestone. The rise in sea level at the base of cycle IIa is referred to as the Taghanic Onlap and recognized by the overlap of the Cedar Valley Limestone over the Wapsipinicon Formation.

METHODS OF STUDY

Eleven outcrops and four cores were selected for this study (Figure 2). The outcrops were chosen on the basis of completeness of section, availability, and location, with emphasis placed on using well-exposed outcrops and type sections. Cores were selected to span the distances between outcrops. A total of 1920 thin sections were analyzed from 437.4 meters of vertical section, giving an average vertical spacing of 22.8 centimeters. Outcrop and core locations were described by Kocken (1989).

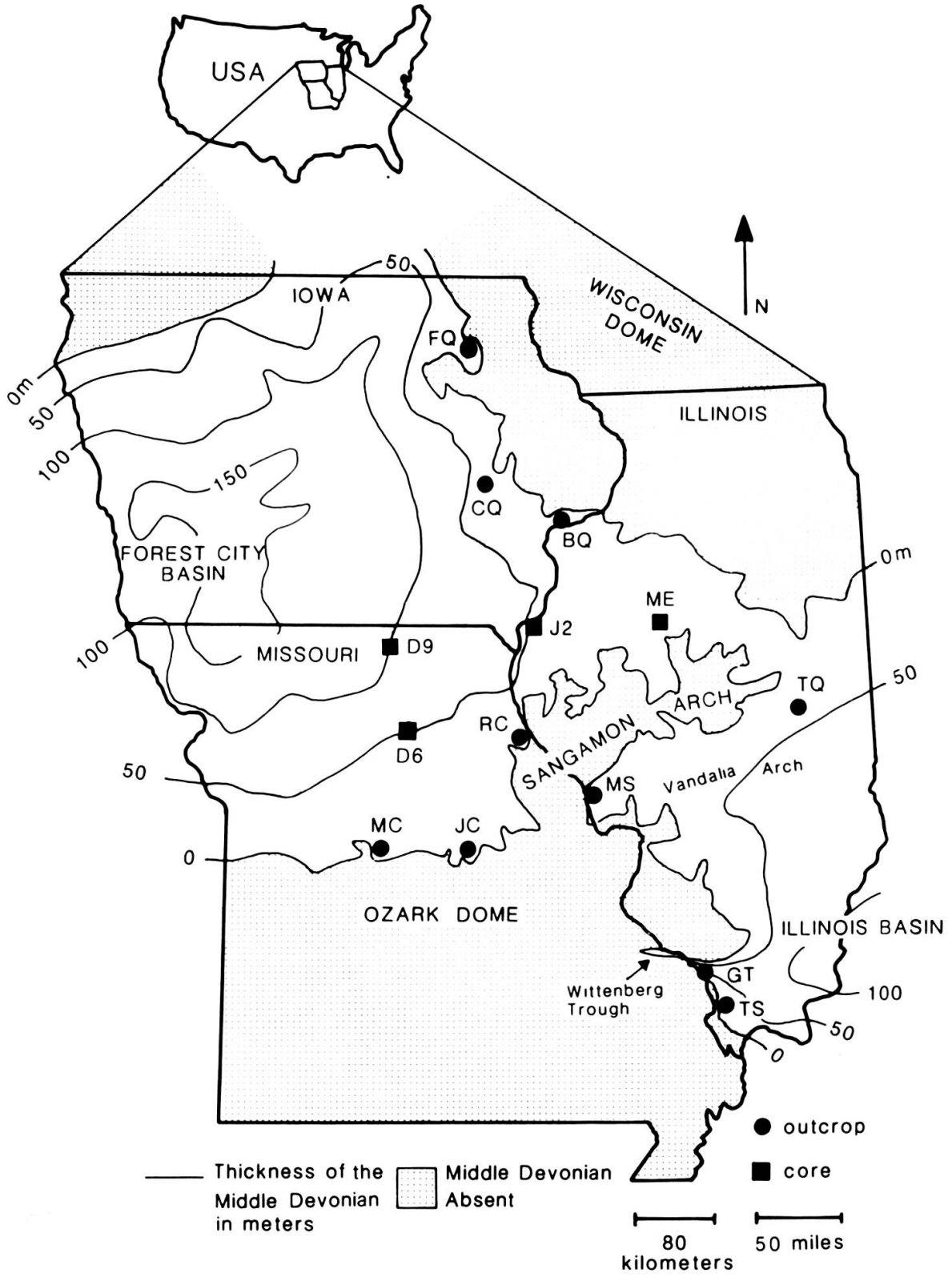

FIG. 2.

Index map of sample localities with thickness of Middle Devonian and major structural features (modified from Collinson and others,1967).

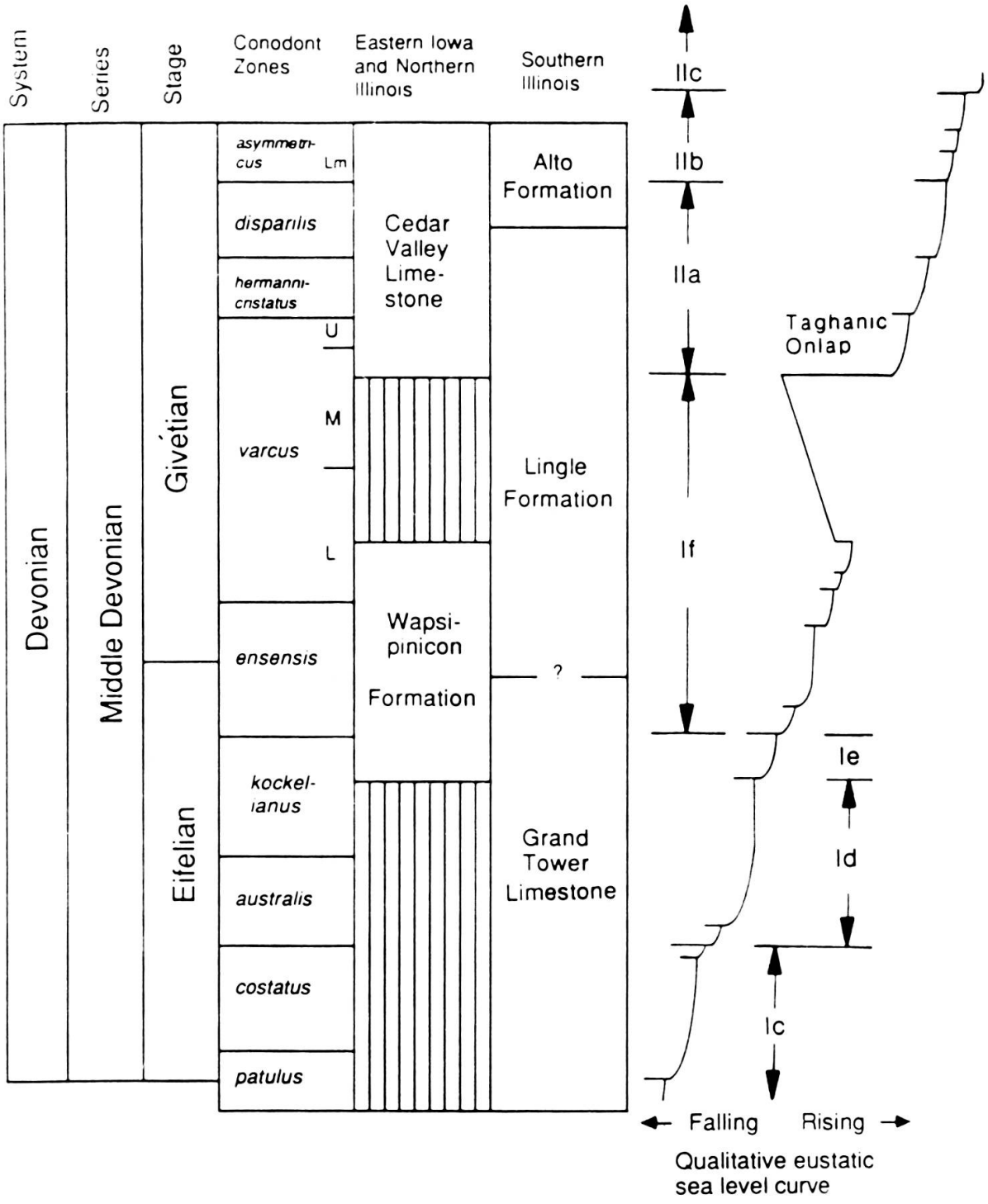

FIG. 3.

Qualitative sea level chart for the Middle Devonian (modified from Johnson and others,1985).

The microfacies techniques recently reviewed in detail by Carozzi (1989) were applied to this study. Thin sections were first divided into preliminary microfacies based on textural characteristics, bioclasts and inorganic components which separated groups according to the depositional energy as reflected in the amount of matrix and cement, with a secondary division based on bioclasts. Indices of clasticity and frequencies were measured for ooids, quartz, intraclasts, oncoids, fecal pellets and crinoids. Frequencies were recorded for brachiopods, bryozoans, ostracods, corals, gastropods, bivalves, stromatoporoids, trilobites, charophyte algae, and calcispheres. Visual estimations were also done of the percent dolomite, cement, matrix, bioclasts, intraclasts, quartz grains, stromatolites and evaporite pseudomorphs. Dolomite crystal size was measured and recorded. Other features such as glauconite, plant spores, types of stromatoporoids (tabular, encrusting, bulbous, and domal), bioturbation and fenestral fabric were indicated as being either rare (<< 1%), present (< 1 %), common (1 - 10 %), or abundant (> 10 %).

Frequency measurements represent the total number of a given component occurring in six adjacent fields of view of the thin section under low power (20 X), corresponding to an area of 380 square millimeters. Calcispheres and fecal pellets were counted at medium power (100 X) over an area of 15.2 square millimeters. The size limit between matrix and bioclast was set at 60 microns because of the difficulty in accurately identifying bioclasts smaller than this size. Clasticity indices and dolomite crystal size (in millimeters) were obtained by measuring the maximum diameters of the largest grains or crystals in each of the six fields of view and then calculating the mean value. The clasticity index closely represents bed shear energy level of currents or degree of agitation in the depositional environment. Frequency values of nontransported components, such as corals and stromatoporoids, provide information on paleoecology. Frequency values of readily transported components, such as quartz and crinoids, give information on the load being transported by currents.

Compared to previous statistical treatments of microfacies (see Carozzi,1989), a new technique was used in this study, namely the DISCRIM procedure of SAS (SAS, 1987a and b) on the IBM 4341 computer under the CMS operating system at the University of Illinois. The DISCRIM procedure generates a final classification of thin sections into distinct microfacies for each depositional model; it allows calculation of final averages per microfacies; and through the CORR procedure it calculates Pearson Correlation Coefficients of microfacies for each depositional model (see Kocken, 1989 for details).

Ideal shallowing-upward sequences were developed by studying the vertical sequences of microfacies seen in cores and outcrops and by using the statistical relationships between microfacies. Sequences in the cores and outcrops are generally incomplete and ideal shallowing-upward sequences could only be constructed by combining several vertical sections. After an ideal shallowing-upward sequence was developed it was interpreted horizontally as a depositional model according to Walther's Law (Middleton, 1973).

DESCRIPTION OF NORMAL MARINE MICROFACIES

The petrographic study resulted in the separation of the thin sections into two main divisions: fossiliferous normal marine microfacies and hypersaline microfacies. The normal marine samples were divided into 12 microfacies, numbered from 1 to 12 in a shoreward direction. They belong to the Grand Tower Limestone and Lingle Formation, south of the Sangamon Arch, and to the Cedar Valley Limestone, north of the Sangamon Arch.

DESCRIPTION OF MICROFACIES

Microfacies 1 (Plate 1, A)

Fossiliferous, bioturbated, slightly argillaceous calcisiltite with scattered, less than 10 percent, sand-sized bioclasts of crinoids, bryozoans, brachiopods, and ostracods.

Microfacies 2 (Plate 1, B)

Bioturbated calcisiltite-supported biocalcarenite with 10 to 30 percent, poorly-sorted, sand-sized bioclasts of brachiopods, crinoids and bryozoans.

Microfacies 3 (Plate 1, C)

Grain-supported to pressure-welded bioclastic calcarenite with greater than 30 percent, sand-sized bioclasts of brachiopods, crinoids, and bryozoans and calcisiltite matrix. Individual corals and stromatoporoids can be locally abundant forming biostromes. The highly bioturbated matrix is slightly bituminous with scattered pyrite crystals. Calcisiltite intraclasts are derived from microfacies 3 and 4.

Microfacies 4 (Plate 1, D)

Grain-supported, slightly pressure-welded bioclastic calcarenite with more than 30 percent sand-sized bioclasts and an association of calcisiltite matrix and minor calcite overgrowth cement on crinoids. Dominant bioclasts are crinoids, brachiopods and bryozoans with lesser trilobites and ostracods. Individual corals and stromatoporoids are locally abundant forming biostromes. Calcisiltite intraclasts are derived from microfacies 3 and 4.

Microfacies 5 (Plate 1, E)

Grain-supported to pressure-welded bioclastic calcarenite with calcite pore-filling or overgrowth cement and minor bioclastic calcisiltite matrix. Bioclasts are moderately sorted with predominant crinoids, brachiopods, and bryozoans.

PLATE 1

Normal Marine Microfacies

A. Microfacies 1; B. Microfacies 2; C. Microfacies 3; D. Microfacies 4; E. Microfacies 5; F. Microfacies 6; G. Microfacies 7; H. Microfacies 8. See text for detailed description. All photomicrographs: plane polarized light.

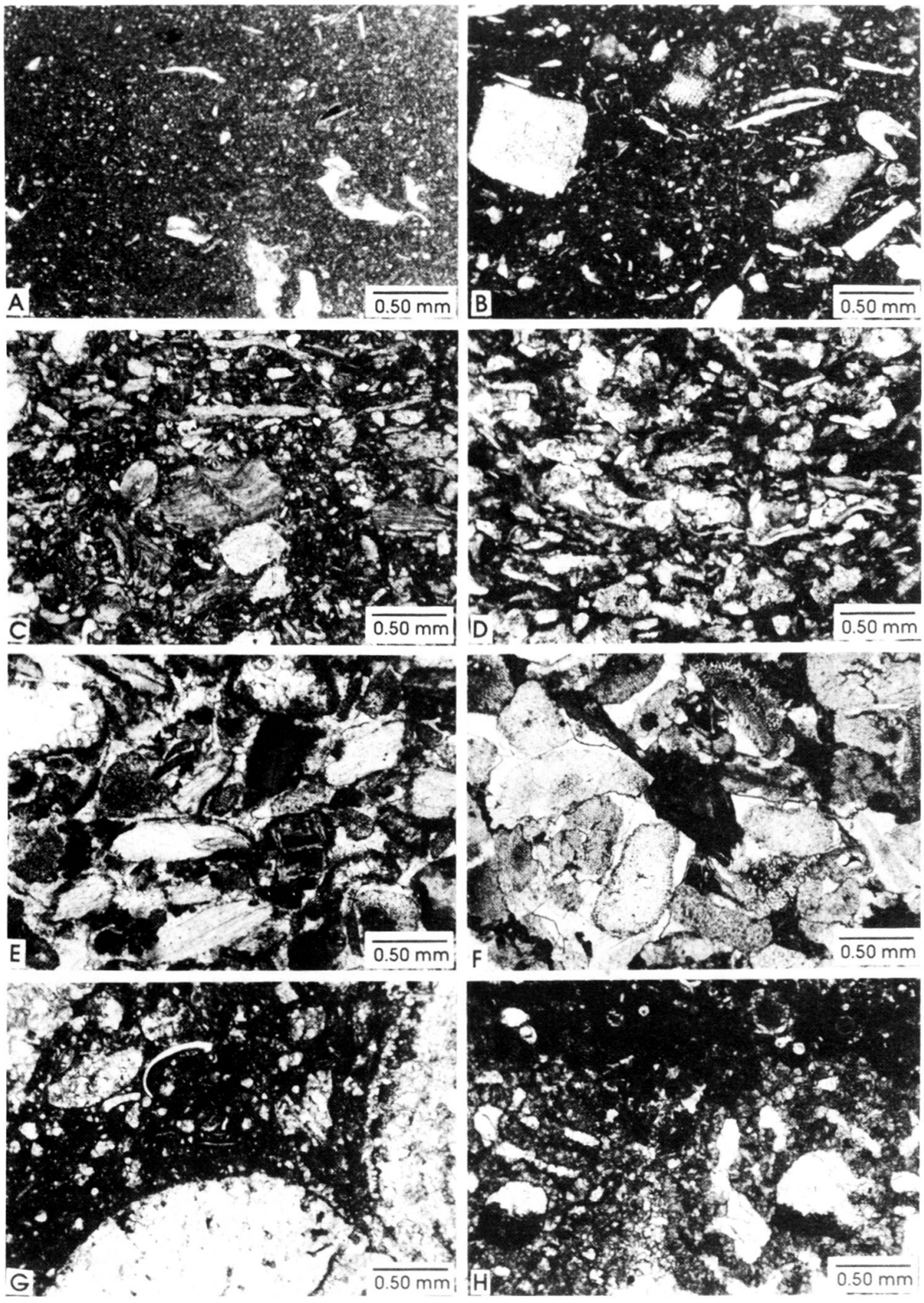
A
0.50 mm
B
0.50 mm
C
0.50 mm
D
0.50 mm
E
0.50 mm
F
0.50 mm
G
0.50 mm
H
0.50 mm

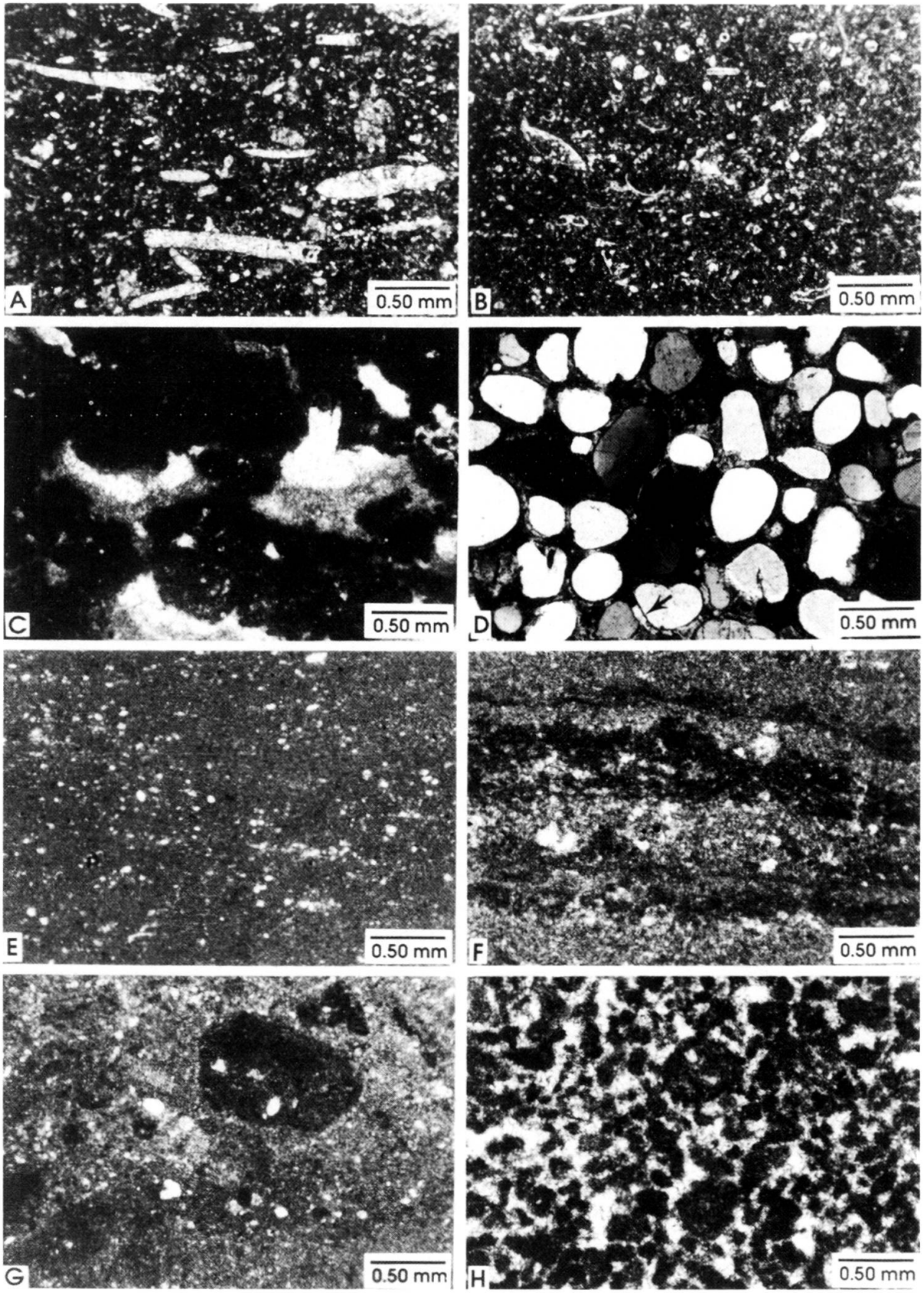
A
0.50 mm
B
0.50 mm
C
0.50 mm
D
0.50 mm
E
0.50 mm
F
0.50 mm
G
0.50 mm
H
0.50 mm

Microfacies 6 (Plate 1, F)

Grain-supported to partly pressure-welded, moderately- to well-sorted, bioclastic calcarenite with pore-filling or overgrowth sparite cement. Common bioclasts are crinoids, bryozoans and brachiopods. Intraclasts are derived from microfacies 6 or 8.

Microfacies 7 (Plate 1, G)

Branching to massive stromatoporoid-constructed limestone. Interstitial material is a calcisiltite-supported calcarenite with common bioclasts of corals, stromatoporoids and ostracods.

Microfacies 8 (Plate 1, H)

Amphipora-accumulated limestone with fossiliferous calcisiltite matrix and rare calcite cement. Matrix is locally bituminous, pelletoidal or fenestral. Other bioclasts include stromatoporoids (mat types) ostracods, calcispheres, brachiopods, and corals.

Microfacies 9 (Plate 2, A)

Slightly bioturbated to laminated, bituminous, fossiliferous calcisiltite with scattered sand-sized bioclasts of stromatoporoids and dasycladaceae algae (*Beresellaceae*). Stromatoporoids are *Amphipora* or mat types.

Microfacies 10 (Plate 2, B)

Light-colored, slightly bioturbated fossiliferous calcisiltite to calcisiltite-supported calcarenite with common ostracods and calcispheres.

Microfacies 11 (Plate 2, C)

Fenestral, grain-supported intraclastic calcarenite with merged pelletoidal calcisiltite matrix to fenestral, pelletoidal calcisiltite with calcispheres and ostracods. Oncolites and detrital quartz are locally abundant. Fenestral fabric can comprise up to 30 percent of the rock and is commonly filled with vadose silt, sparite cement or a combination of both.

Microfacies 12 (Plate 2, D)

Medium-grained, grain-supported quartz arenite with sparite cement and minor calcisiltite matrix. Quartz grains are usually well-sorted and well-rounded with predominantly straight extinctions, and could be reworked from the Ordovician St. Peter Sandstone. Most quartz grains have corroded margins from replacement by calcite which forms well-developed rings indicating the original outline of the grains (arrow).

PLATE 2

Normal Marine Microfacies (Continued) and Hypersaline Microfacies

A. Microfacies 9; B. Microfacies 10; C. Microfacies 11; D. Microfacies 12; E. Microfacies H1; F. Microfacies H2; G. Microfacies H3; H. Microfacies H4. See text for detailed description. All photomicrographs: plane polarized light, except D: crossed nicols.

MODEL 1. NORMAL MARINE ENVIRONMENT, SOUTH OF THE SANGAMON ARCH

INTRODUCTION

Model 1 (Figures 4 and 5) represents the normal open marine depositional environment south of the Sangamon Arch and corresponds to the Grand Tower Limestone and Lingle Formation. It is a gentle carbonate ramp that extends from a quartz sand beach offshore to a basinal setting with no distinct break in slope. There is no evidence of bioconstructed, bioaccumulated or hydrodynamic buildups. Only microfacies 1 through 6 and 12 are present. Microfacies 7 through 11 were not found in any sections south of the Sangamon Arch. The model consists of a continuous series of microfacies, ranging from a pure quartz arenite with calcite cement representing a beach and highest energy (microfacies 12), through grain-supported biocalcarenites with calcite cement representing the shallowest subtidal zone and high energy (microfacies 6), to unfossiliferous calcisiltites corresponding to the deepest water and lowest energy (microfacies 1). This model is divided into four environments: beach (microfacies 12), upper ramp (microfacies 5 and 6), lower ramp (microfacies 3 and 4), and basinal (microfacies 1 and 2).

COMPONENT VARIATIONS

Components (Figure 5) are divided into two groups: transported downslope and accumulated in place.

In the first group, quartz shows a constant supply with a linear parallel decrease of clasticity and frequency from the quartz sand beach to the basinal environment. Intraclasts were generated in the upper ramp (microfacies 6) and distributed by currents in all directions up- and downslope. Crinoid colonies developed in the upper ramp (microfacies 5 and 6). Their abraded bioclasts were transported by currents downslope with a behavior of clasticity and frequency similar to those of detrital quartz. Minor fluctuations of crinoid clasticity in the lower ramp and basinal environments indicate local supplies from small crinoid colonies producing bioclasts larger than those transported. The behavior of bryozoans is similar to that of crinoids, but some of the bryozoans found in the deeper environments are delicate forms representing in place colonies. Ostracods lived in the upper ramp environment and their disarticulated tests were transported into the lower ramp and basinal environments.

In the second group, trilobites occur in the upper and lower ramp. Brachiopods reached peak frequency in the upper part of the lower ramp whereas relatively rare stromatoporoids and corals show respectively upper ramp and lower-upper ramp preferred location of growth.

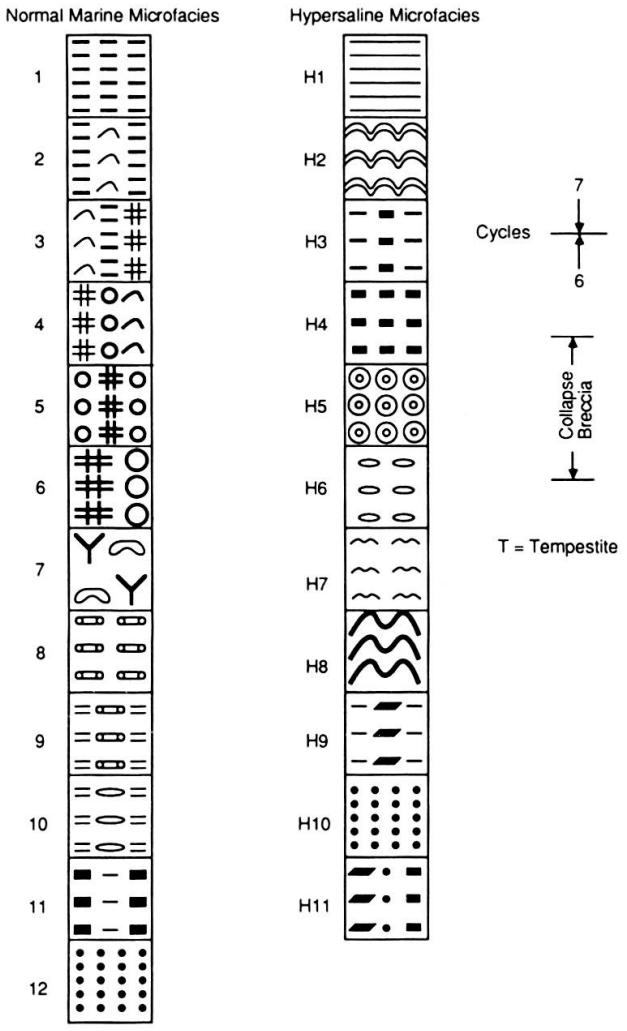

FIG.4.

Symbols used in depositional models and stratigraphic sections

Percent matrix, cement, bioclasts, and intraclasts represent various expressions of the decrease in depositional energy from quartz sand beach to basinal environment.

Authigenic glauconite is concentrated in pores of crinoids and zooecia of bryozoans of basinal and lower-upper ramp microfacies. It rarely replaces the calcite framework of bioclasts. A very small amount of rounded grains of detrital glauconite occurs associated with detrital quartz and intraclasts in the above-mentioned microfacies.

Intensity of bioturbation increased uniformly from the upper ramp to the basinal environment. Dolomite present in all three zones suggests an origin from pervasive burial dolomitization related to fluids expelled by burial shale compaction or by basinal fluid flow.

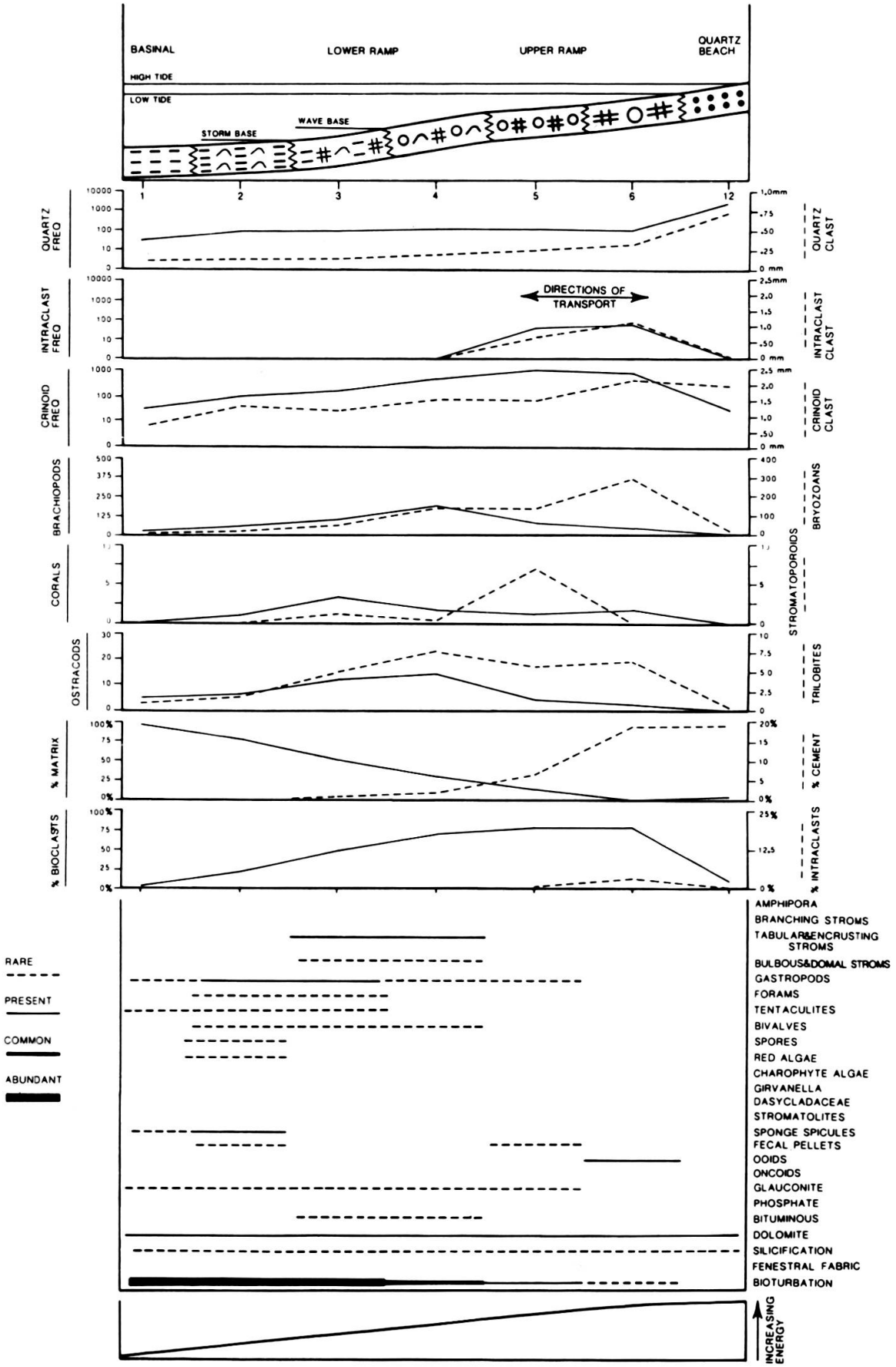
BASINAL
LOWER RAMP
UPPER RAMP
QUARTZ BEACH
HIGH TIDE
LOW TIDE
STORM BASE
WAVE BASE
1
2
3
4
5
6
12
QUARTZ FREQ
QUARTZ CLAST
INTRACLAST FREQ
INTRACLAST CLAST
DIRECTIONS OF TRANSPORT
CRINOID FREQ
CRINOID CLAST
BRACHIOPODS
BRYOZOANS
CORALS
STROMATOPOROIDS
OSTRACODS
TRILOBITES
% MATRIX
% CEMENT
% BIOCLASTS
% INTRACLASTS
AMPHIPORA
BRANCHING STROMS
TABULAR&ENCRUSTING STROMS
BULBOUS&DOMAL STROMS
GASTROPODS
FORAMS
TENTACULITES
BIVALVES
SPORES
RED ALGAE
CHAROPHYTE ALGAE
GIRVANELLA
DASYCLADACEAE
STROMATOLITES
SPONGE SPICULES
FECAL PELLETS
OOIDS
ONCOIDS
GLAUCONITE
PHOSPHATE
BITUMINOUS
DOLOMITE
SILICIFICATION
FENESTRAL FABRIC
BIOTURBATION
RARE
PRESENT
COMMON
ABUNDANT
INCREASING ENERGY

MODEL 2. NORMAL MARINE ENVIRONMENT, NORTH OF THE SANGAMON ARCH

INTRODUCTION

Model 2 (Figure 6) represents the normal marine depositional environment north of the Sangamon Arch and corresponds to the Cedar Valley Limestone. This model is a carbonate platform with a frontal stromatoporoid buildup. The model is divided into five environments: intertidal flat (microfacies 11), ecologically zoned lagoon (microfacies 8, 9 and 10), stromatoporoid buildup (microfacies 7), slope (microfacies 3, 4, 5 and 6), and basinal (microfacies 1 and 2). The intertidal flat consists mainly of fenestral calcisiltites and fenestral intraclastic calcarenites with pelletoidal calcisiltite matrix. The low-energy lagoon consists of three juxtaposed subenvironments represented by a fossiliferous calcisiltite with ostracods and calcispheres next to the intertidal flat, a bituminous, fossiliferous calcisiltite in the middle, and an *Amphipora*-accumulated limestone next to the buildup. The stromatoporoid buildup has a framework of branching and massive stromatoporoids with an interstitial calcisiltite-supported calcarenite. The slope grades from a grain-supported biocalcarenite with calcite cement next to the buildup, to a grain-supported biocalcarenite with calcisiltite matrix next to the basinal environment. The basinal environment consists of calcisiltite-supported calcarenites and fossiliferous calcisiltites.

COMPONENT VARIATIONS

Components (Figure 6) are divided into two groups: transported downslope and accumulated in place.

In the first group, quartz originating from the intertidal flat was effectively trapped in the shoreward part of the lagoon, it bypassed the stromatoporoid ridge where it was cut by tidal channels, and its finest grains settled in the middle slope to basinal environments. The three peaks of frequency and clasticity of intraclasts indicate areas of their generation surrounded by zones of short transportation. Intraclasts in the intertidal flat are reworked calcisiltite desiccation chips, those of the two other zones are fossiliferous calcisiltites. The larger size of intraclasts in the upper slope compared with the basinal and lagoonal environments reflects the maximum reworking energy in front of the stromatoporoid buildup. Crinoids occur in two distinct populations: relatively rare and small species in the lagoon with no appreciable transportation of their bioclasts, abundant and large species in the upper slope with basinward transportation of their bioclasts. Bryozoan colonies preferentially grew in the lower slope, just below wave

FIG. 5

Model 1. Normal marine, south of the Sangamon Arch.

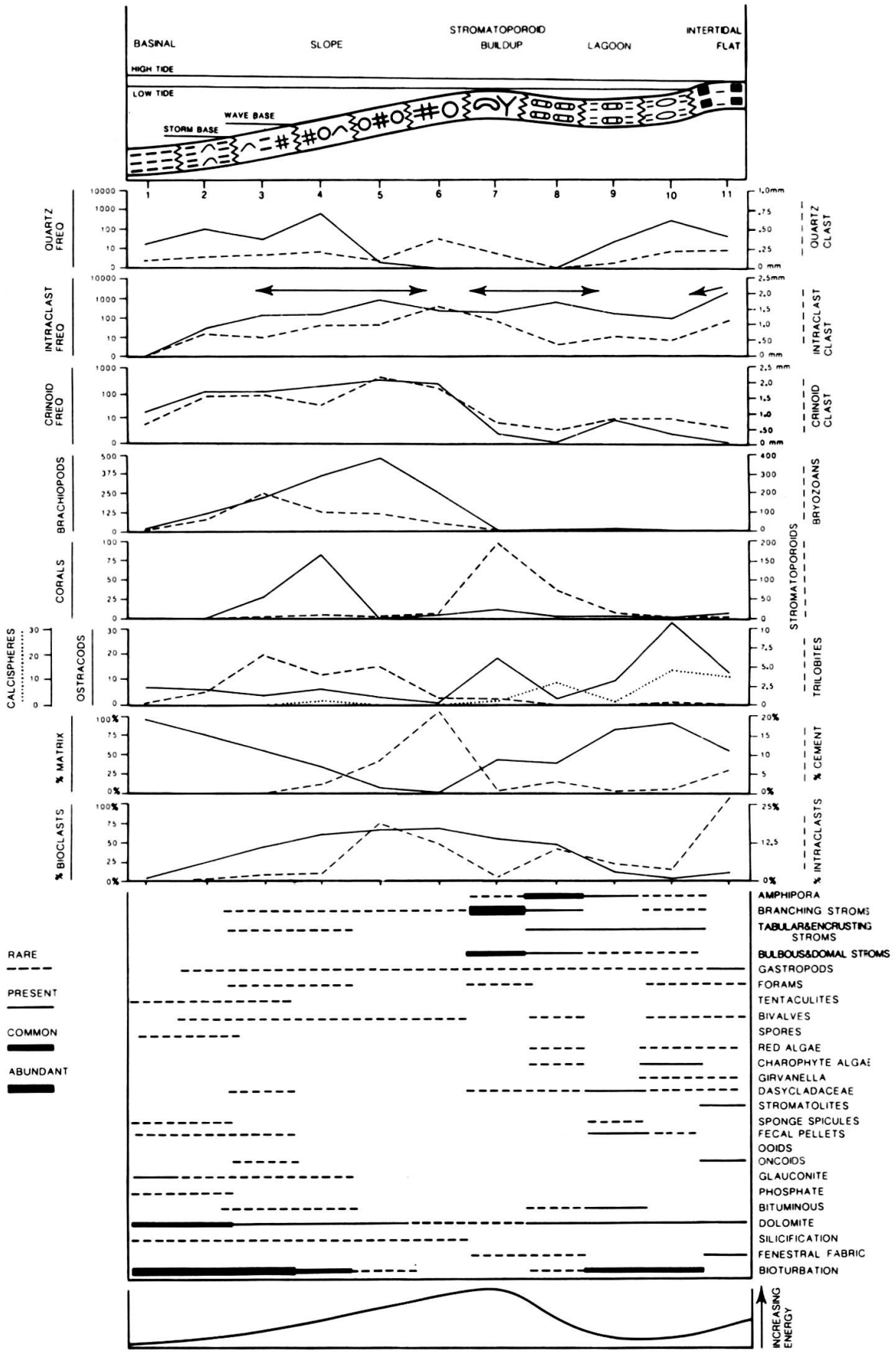
BASINAL
SLOPE
STROMATOPOROID BUILDUP
LAGOON
INTERTIDAL FLAT
HIGH TIDE
LOW TIDE
WAVE BASE
STORM BASE
1 2 3 4 5 6 7 8 9 10 11
QUARTZ FREQ
QUARTZ CLAST
INTRACLAST FREQ
INTRACLAST CLAST
CRINOID FREQ
CRINOID CLAST
BRACHIOPODS
BRYOZOANS
CORALS
STROMATOPOROIDS
CALCISPHERES
OSTRACODS
TRILOBITES
% MATRIX
% CEMENT
% BIOCLASTS
% INTRACLASTS
RARE
PRESENT
COMMON
ABUNDANT
AMPHIPORA
BRANCHING STROMS
TABULAR&ENCRUSTING STROMS
BULBOUS&DOMAL STROMS
GASTROPODS
FORAMS
TENTACULITES
BIVALVES
SPORES
RED ALGAE
CHAROPHYTE ALGAE
GIRVANELLA
DASYCLADACEAE
STROMATOLITES
SPONGE SPICULES
FECAL PELLETS
OOIDS
ONCOIDS
GLAUCONITE
PHOSPHATE
BITUMINOUS
DOLOMITE
SILICIFICATION
FENESTRAL FABRIC
BIOTURBATION
INCREASING ENERGY

base, and their abraded bioclasts were distributed mainly in an upper slope direction. Ostracods and calcispheres were abundant in the lagoon and their bioclasts transported basinward and frequently trapped in the interstices of the stromatoporoid buildup.

In the second group, trilobites occur in the slope environment whereas brachiopods reach their maximum frequency between middle and upper slope. The stromatoporoid buildup consisted of branching, massive, and bulbous forms with related bioclasts. The rare stromatoporoids of the lagoon were mainly *Amphipora* and thin tabular forms. A few colonies of stromatoporoids in the middle slope are associated with thin rugose coral biostromes with *Hexagonaria* developed at wave base. The corals in the lagoon and in the stromatoporoid buildup are mainly tabulate.

Percent of matrix, cement, bioclasts, and intraclasts represent various expressions of the depositional energy level which reaches its peak at the stromatoporoid buildup.

Authigenic and detrital glauconite occur in the same habits as in model 1, in basinal and slope microfacies. Bioturbation is extensive both in the lagoon and in the basinal environment. Dolomite present in all zones is interpreted as in model 1.

DESCRIPTION OF HYPERSALINE MICROFACIES

Hypersaline microfacies and related depositional models pertain to the Wapsipinicon Formation, Geneva Dolomite Member of the Grand Tower Limestone, and Cooper Lithofacies of the Cedar Valley Limestone. The lack of normal marine fossils along with the presence of stromatolites, very finely crystalline to aphanocrystalline dolomite, collapse breccias, desiccation cracks, exposure features, gypsum and anhydrite pseudomorphs are characteristic of the hypersaline microfacies. In collapse breccias, petrographic studies pertain to the clasts in the samples and not to interstitial cement or matrix. Thus, microfacies assignments were based only on the nature of the clasts with the understanding that the collapse process could disrupt the vertical sequence. Hypersaline microfacies were divided into eleven microfacies, labeled H1 to H11 in a general shoreward direction.

DESCRIPTION OF MICROFACIES

Microfacies H1 (Plate 2, E)

Slightly laminated to massive, light-colored, unfossiliferous and quartz-silty calcisiltite with a few scattered thin-shelled ostracods and fecal pellets; and very rare

FIG. 6.

Model 2. Normal marine, north of the Sangamon Arch.

calcispheres, dasycladaceae algae and brachiopods. Calcite pseudomorphs after gypsum are rare.

Microfacies H2 (Plate 2, F)

Stromatolite-constructed limestone with occasional desiccation cracks and fenestral fabric. Stromatolites typically consist of darker superposed mats separated by a lighter colored pelletoidal calcisiltite matrix. Individual mats vary from well preserved to very disrupted and desiccated, with some local pelletization. Fenestrae and desiccation cracks are usually filled with calcite cement.

Microfacies H3 (Plate 2, G)

Calcisiltite-supported intraclastic calcarenite with rare fenestral fabric and intercalated stromatolite mats. Intraclasts are poorly sorted and subangular, and consist of dark-colored, unfossiliferous calcisiltite. Stromatolite mats are disrupted and thin. Fenestrae are filled with calcite cement and/or vadose silt. Calcite pseudomorphs after gypsum and anhydrite are rare.

Microfacies H4 (Plate 2, H)

Grain-supported intraclastic to lithic pelletoidal calcarenite with microsparite cement and calcisiltite matrix. Intraclasts are generally subrounded, moderately sorted, and similar to those in H3. Calcite pseudomorphs after gypsum and anhydrite are rare.

Microfacies H5 (Plate 3, A)

Grain-supported oolitic calcarenite with microsparite calcite cement. Ooids are moderately sorted. The cores of the ooids are rounded, unfossiliferous calcisiltite intraclasts similar in composition to intraclasts in H3 and H4. Half-moon ooids are common, having resulted from the dissolution of more soluble (evaporitic ?) concentric laminae (Carozzi, 1963). Oomoldic porosity is common and resulted from burial dissolution. The ooids and calcite cement are often extensively neomorphosed to microspar, with some ooids visible only as ghosts.

Microfacies H6 (Plate 3, B)

Ostracod-accumulated limestone with organic-rich pelletoidal calcisiltite matrix. Ostracods are predominantly thick-shelled forms with irregular shapes. The calcisiltite matrix is typically light yellow in color with scattered pyrite crystals. Kerogen occurs as orange to brown colored translucent material, commonly concentrated along laminae.

PLATE 3

Hypersaline Microfacies (continued)

A. Microfacies H5; B. Microfacies H6; C. Microfacies H7; D. Microfacies H8; E. and F. Microfacies H9; G. Microfacies H10; H. Microfacies H11. See text for detailed description. All photomicrographs: plane polarized light, except G: crossed nicols.

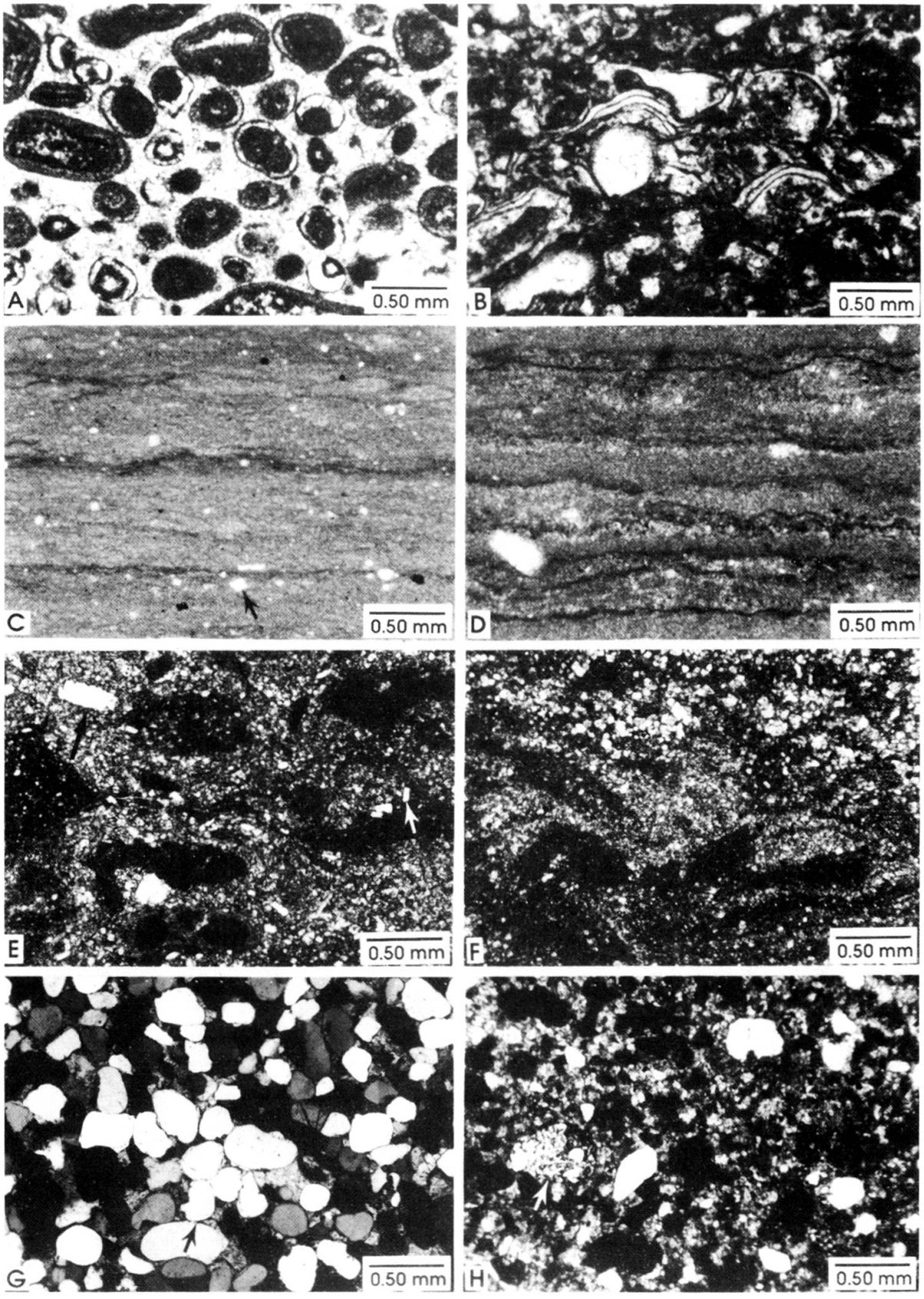
A
0.50 mm
B
0.50 mm
C
0.50 mm
D
0.50 mm
E
0.50 mm
F
0.50 mm
G
0.50 mm
H
0.50 mm

Microfacies H7 (Plate 3, C)

Slightly laminated pelletoidal, pyritic, organic-rich calcisiltite. Laminae are wavy and irregular. A few thick-shelled ostracods are present. Kerogen is orange to brown in color and occurs mainly between the laminae. Dedolomitization consisting of rhombic shapes filled with microspar (arrow), is locally abundant. Calcite pseudomorphs after gypsum and anhydrite are rare.

Microfacies H8 (Plate 3, D)

Organic-rich stromatolite-constructed limestone, similar to H2, but bituminous.

Microfacies H9 (Plate 3, E and F)

Partially dolomitized, grain-supported to calcisiltite-supported intraclastic calcarenite with calcisiltite matrix. Angular and poorly-sorted intraclasts due to desiccation consist of unfossiliferous, very finely crystalline to aphanocrystalline dolomite or unfossiliferous calcisiltites. Detrital quartz, vadose silt, fenestral fabric and quartz pseudomorphs after gypsum and anhydrite (arrows) are present. Stromatolites are rare, thin and often dolomitized. This microfacies typically occurs in collapse breccias.

Microfacies H10 (Plate 3, G)

Fine- to medium-grained quartz arenite. Quartz is usually well sorted and well rounded, with straight extinctions predominant over wavy. A bimodal size distribution occurs locally. Carbonate intraclasts and reworked chert clasts are rare. Interstitial material is either poikilotopic sparite cement, coarse sparite cement, coarse-grained dolomite, or calcisiltite. Quartz overgrowths are common. Some quartz grains are marginally replaced by carbonates (arrow).

Microfacies H 11 (Plate 3, H)

Grain-supported, intraclastic, arenaceous calcarenite with calcisiltite matrix. Intraclasts consist of dark unfossiliferous calcisiltites and very finely crystalline to aphanocrystalline dolomites. Intraclasts are subrounded and moderately sorted. Reworked (Silurian or Ordovician) chert clasts are common. Phosphate pellets (arrow) are rounded and rare, having resulted from local reworking. This microfacies occurs in thin beds and is interpreted as representing submarine erosion and reworking of both older formations and local contemporaneous sediments.

Two depositional models were constructed from the statistical analysis and vertical succession of hypersaline microfacies. Model 3 is typically bituminous and consists of microfacies H6, H7, H8, H9, and H10. Model 4 is nonbituminous and consists of microfacies H1, H2, H3, H4, H5, H9, and H10. Microfacies H9 and H10 are

FIG. 7.

Model 3. Partly anoxic hypersaline environment.

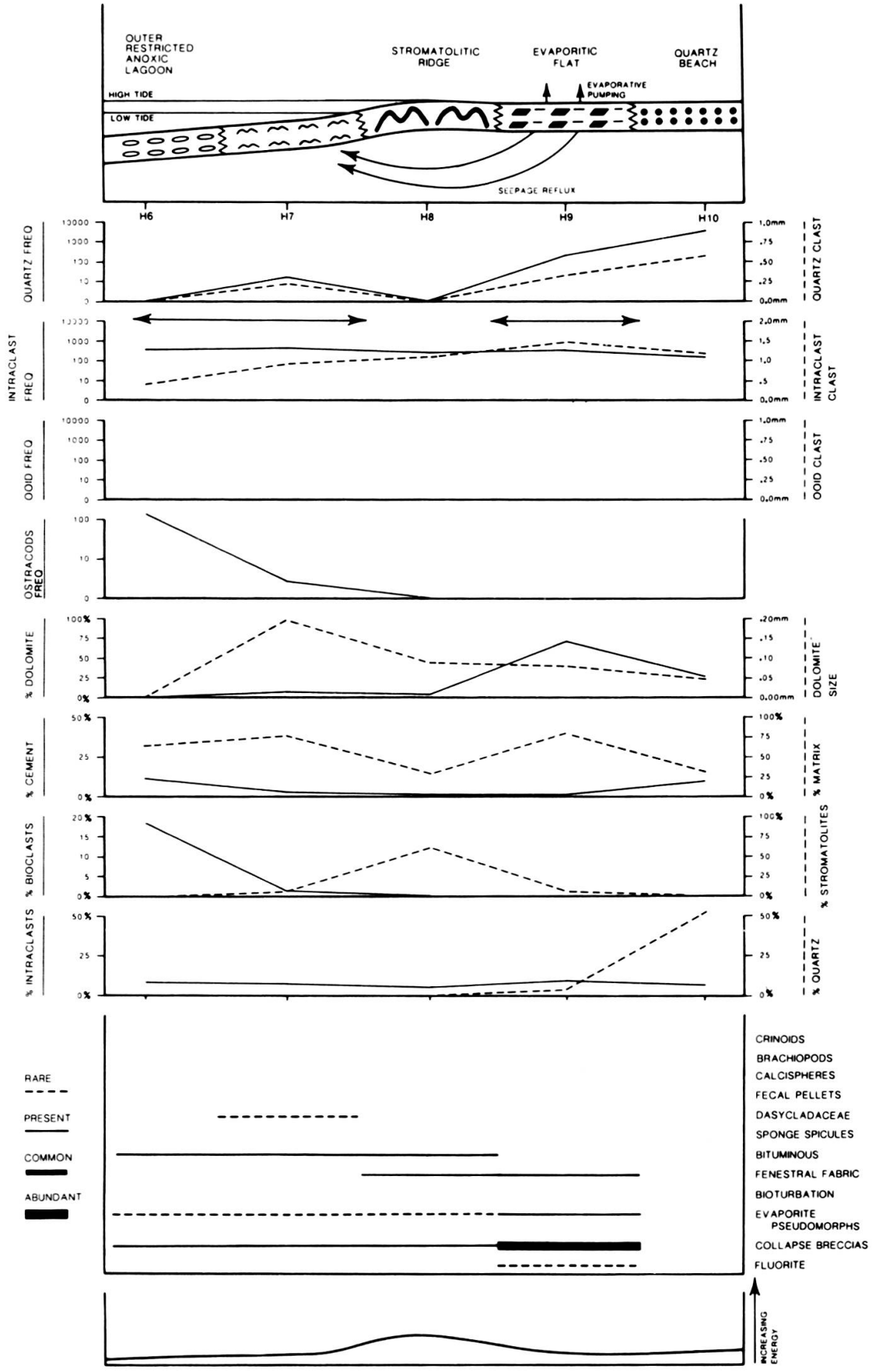
OUTER RESTRICTED ANOXIC LAGOON
STROMATOLITIC RIDGE
EVAPORITIC FLAT
QUARTZ BEACH
HIGH TIDE
LOW TIDE
EVAPORATIVE PUMPING
SEEPAGE REFLUX
H6
H7
H8
H9
H10
QUARTZ FREQ
QUARTZ CLAST
INTRACLAST FREQ
INTRACLAST CLAST
OOID FREQ
OOID CLAST
OSTRACODS FREQ
% DOLOMITE
DOLOMITE SIZE
% CEMENT
% MATRIX
% BIOCLASTS
% STROMATOLITES
% INTRACLASTS
% QUARTZ
RARE
PRESENT
COMMON
ABUNDANT
CRINOIDS
BRACHIOPODS
CALCISPHERES
FECAL PELLETS
DASYCLADACEAE
SPONGE SPICULES
BITUMINOUS
FENESTRAL FABRIC
BIOTURBATION
EVAPORITE PSEUDOMORPHS
COLLAPSE BRECCIAS
FLUORITE
INCREASING ENERGY

petrographically similar and occur in both models. Vertical positions of H9 and H10 in the outcrops and cores were used to determine whether a thin section belonged to Model 3 or Model 4. Model 3 is commonly overlain by model 4 in several of the vertical sequences, thereby demonstrating a change in the depositional environment from anoxic to more oxygenated.

MODEL 3. PARTLY ANOXIC HYPERSALINE ENVIRONMENT

INTRODUCTION

Model 3 (Figure 7) represents a hypersaline, partially anoxic environment consisting seaward of: quartz sand beach (microfacies 10), evaporitic flat (microfacies H9), stromatolitic ridge (microfacies H8), and outer restricted anoxic lagoon (microfacies H6 and H7). Microfacies H6, H7 and H8 are organic-rich; microfacies H9 and H10 are normal microfacies because of frequent subaerial exposure. The quartz sand beach consists of quartz grains with rare carbonate intraclasts. The evaporitic flat contains dolomitized intraclasts and has common fenestral structures and evaporite pseudomorphs. The stromatolitic ridge consists of bituminous stromatolites. The outer restricted anoxic lagoon shows bituminous pelletoidal calcisiltites with locally abundant thick-shelled ostracods. This model is applicable only to the Kenwood and Spring Grove Members of the Wapsipinicon Formation. Model 3 is always overlain by model 4.

COMPONENT VARIATIONS

Components (Figure 7) are divided into two groups: transported in part downslope or accumulated in place.

In the first group, detrital quartz, originating from the beach, shows transport to the anoxic lagoon and a constant supply is indicated by a parallel decrease of clasticity and frequency. It bypassed the stromatolite ridge through tidal channels. Intraclasts are of two types and underwent short transportation. In the stromatolite ridge and the evaporitic flat, they are abundant and large, consisting of desiccation chips of unfossiliferous slightly dolomitized calcisiltites. In the outer lagoon, intraclasts are smaller fragments formed by submarine reworking of bituminous unfossiliferous calcisiltites.

In the second group, thick-shelled ostracods characterize the deepest part of the lagoon and the percent of stromatolites indicates the bioconstructed ridge.

Percent cement, matrix, and quartz are various expressions of the generally low depositional energy which reaches a small peak at the stromatolite ridge. The percent dolomite curve has a maximum in the evaporitic flat and quartz beach where dolomi-

tization occurred in a sabkha-like environment by evaporative pumping. The stromatolitic ridge and lagoon contain only small amounts of dolomite produced by a weak seepage reflux process. Dolomite rhomb size is largest near the edge of the lagoon and decreases shoreward reflecting that larger dolomite crystals were produced by seepage refluxion compared to evaporative pumping. The evaporitic flat was the site of halite precipitation which upon dissolution generated abundant collapse breccias.

MODEL 4. HYPERSALINE ENVIRONMENT WITH INNER LAGOON

INTRODUCTION

Model 4 (Figure 8) represents a hypersaline environment consisting of : quartz beach (microfacies H10), evaporitic flat (H9), inner lagoon (microfacies H3, H4 and H5), stromatolitic ridge (microfacies H2) and outer restricted lagoon (microfacies H1). The quartz sand beach consists of quartz grains with rare carbonate intraclasts. The evaporitic flat typically contains dolomitized intraclasts, and has common fenestral fabric and gypsum and anhydrite pseudomorphs. The inner lagoon varies from an oolitic calcarenite near the evaporitic flat to a calcisiltite-supported intraclastic calcarenite with intercalated stromatolite mats next to the stromatolitic ridge. The stromatolitic ridge is made of low-relief stromatolites. The outer restricted lagoon consists of light-colored calcisiltites with scattered ostracods and rare brachiopods, dasycladaceae algae, fecal pellets and calcispheres. This lagoon because of the lack of bituminous deposits is not anoxic and is distinct from the outer lagoon in Model 3. Model 4 is applicable to parts of the Wapsipinicon Formation, Geneva Dolomite Member of the Grand Tower Formation, and Cedar Valley Limestone.

COMPONENT VARIATIONS

Components (Figure 8) are divided into two groups: transported or accumulated in place.

In the first group, detrital quartz was transported from beach to outer lagoon with a constant supply indicated by a parallel decrease of clasticity and frequency. It bypassed the oolitic zone and the stromatolitic ridge through tidal channel. Intraclasts are of three distinct types and underwent short transportation. The most effective generation was by desiccation of inner lagoon unfossiliferous calcisiltites, many debris of which formed the cores of ooids. Weaker generation characterized the evaporitic flat with intraclasts of unfossiliferous dolomitized calcisiltites and the outer restricted lagoon with fragments of ostracod calcisiltites.

In the second group, ooid generation is limited to the mildly agitated waters of the inner lagoon whereas thin-shelled ostracods occur in small amount in the outer lagoon and outside portion of the inner lagoon. The percent stromatolites indicates the main constructed ridge and the presence of a few mats in the inner lagoon and the evaporitic flat.

Percent of matrix, cement, bioclasts, intraclasts, and quartz are various expressions of the general very low depositional energy which reaches a small peak at the stromatolitic ridge. The percent dolomite curve has a maximum value in the evaporitic flat. Dolomite in the evaporitic flat and quartz beach was produced by evaporitic pumping and is very finely crystalline to aphanocrystalline. The dolomite in the outer lagoon, stromatolitic ridge, and inner lagoon was probable produced by the mixing of meteoric and marine waters. Rain waters penetrating the stromatolitic ridge and seeping into the inner and outer lagoon produced dolomite by a micro-dorag process (Kaldi and Gidman, 1982). The dolomite size curve has a maximum value in the inner lagoon near the stromatolitic ridge reflecting the larger original grain size of the carbonates in this environment.

The evaporitic flat contains abundant collapse breccias due to the dissolution of halite, less common gypsum and anhydrite pseudomorphs, fenestral structures and rare fluorite. The outer lagoon sediments are commonly bioturbated.

DIAGENESIS OF NORMAL MARINE MICROFACIES

INTRODUCTION

Diagenesis was studied by standard petrographic observation using stained thin sections. Diagenetic sequences are documented by textural relationships and expressed in diagrams (Figures 9 and 10) which show general diagenetic evolution through time. Diagenetic features within each diagenetic environment are not listed in time sequence because they may occur simultaneously. Only significant or unusually diagenetic features are discussed in detail.

Normal marine microfacies display diagenetic features indicating a general evolution starting with marine phreatic and proceeding through marine vadose, meteoric vadose, undersaturated meteoric phreatic, saturated meteoric phreatic, mixed marine-freshwater and ending with burial (Figure 9).

Marine Phreatic

The diagenetic features attributed to this environment are authigenic glauconite, phosphate, pyrite, native sulfur, micrite envelopes, micritization, cyanobacterial coat-

FIG. 8.

Model 4. Hypersaline environment with inner lagoon.

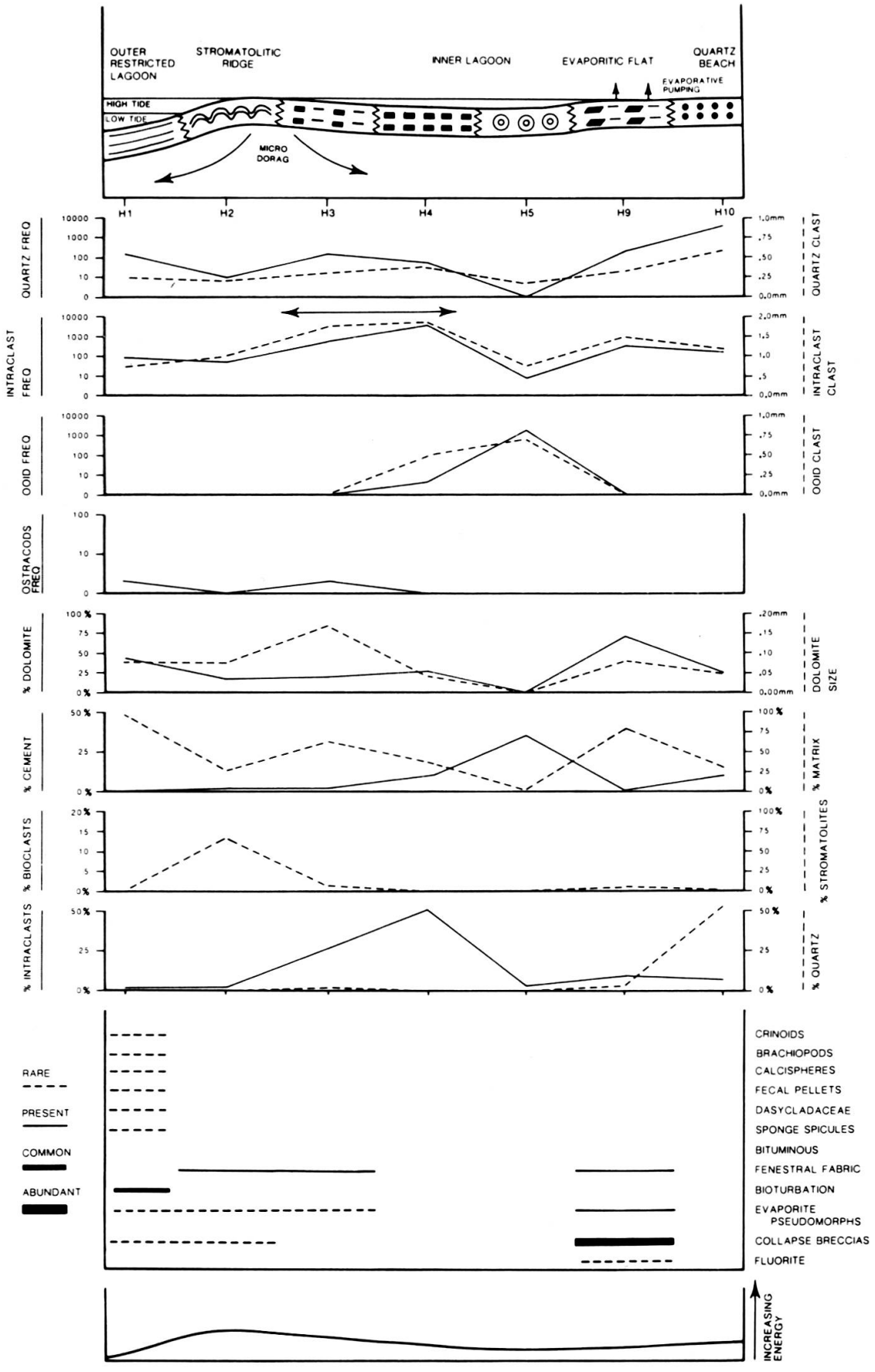
OUTER RESTRICTED LAGOON
STROMATOLITIC RIDGE
INNER LAGOON
EVAPORITIC FLAT
QUARTZ BEACH
EVAPORATIVE PUMPING
HIGH TIDE
LOW TIDE
MICRO DORAG
H1
H2
H3
H4
H5
H9
H10
QUARTZ FREQ
QUARTZ CLAST
INTRACLAST FREQ
INTRACLAST CLAST
OOID FREQ
OOID CLAST
OSTRACODS FREQ
% DOLOMITE
DOLOMITE SIZE
% CEMENT
% MATRIX
% BIOCLASTS
% STROMATOLITES
% INTRACLASTS
% QUARTZ
RARE
PRESENT
COMMON
ABUNDANT
CRINOIDS
BRACHIOPODS
CALCISPHERES
FECAL PELLETS
DASYCLADACEAE
SPONGE SPICULES
BITUMINOUS
FENESTRAL FABRIC
BIOTURBATION
EVAPORITE PSEUDOMORPHS
COLLAPSE BRECCIAS
FLUORITE
INCREASING ENERGY

ings, borings, hardgrounds, early lithification, reworking of intraclasts, silicification (I) (Plate 4, A), compaction (I) and early cementation (Plate 4, B, C and D).

Evidence of early silicification (I) occurs in chert nodules displaying an internal uncompacted texture as compared to the enclosing rock (Carozzi and Gerber, 1978). In particular, plant spores are preserved spherical and unflattened in the chert nodules while flattened outside the nodules (Plate 4, A).

Marine phreatic calcite cements (Plate 4, B, C and D) are radiaxial, fascicular-optic, fibrous isopachous and syntaxial (I). All four occur in minor amounts in microfacies 5, 6 and 8, and are usually overlain by later meteoric phreatic cements. Radiaxial and fascicular optic calcite cements mainly overlie brachiopod shells, where their extinction pattern mimics that of the brachiopods which controlled their nucleation and growth. Fibrous isopachous cement occurs on ooids, intraclasts and bioclasts. Early syntaxial cement (I) develops as inclusion-rich syntaxial overgrowths on crinoids and usually overlain by clear syntaxial cement (II), both in optical continuity with the crinoid. This cement is interpreted as early because it is rich in non-carbonate opaque inclusions, overlain by internal sediment and overgrown by clear syntaxial cement (II).

PLATE 4

Diagenesis of Normal Marine Microfacies

A. Microfacies 3. Silicified, calcisiltite-supported calcarenite with scattered crinoids and brachiopods. Plant spores (arrows) are circular shaped suggesting silicification in marine phreatic environment prior to compaction. B. Microfacies 8. *Amphipora*-accumulated limestone with grain-supported intraclastic calcarenite matrix. Fibrous isopachous rim cement (arrows) occurs on *Amphipora* and intraclasts. Dissolution channel (C) is partially lined with pyrite and filled with sparite cement. C. Microfacies 6. Grain-supported crinoid-brachiopod calcarenite with minor pelletoidal calcisiltite internal sediment (arrows) and two generations of calcite cement. Brachiopod bioclasts (B) are overlain by radiaxial and fascicular optic calcite cements. Crinoids are surrounded by syntaxial (I) cement rich in noncarbonate opaque inclusions. The presence of internal sediment (arrows) on top of the cements demonstrates their origin in marine phreatic environment. A second generation of sparite overlies early cements and internal sediment. D. Microfacies 6. Grain-supported crinoid-brachiopod calcarenite with two generations of syntaxial cement on crinoids and fascicular optic calcite cements on brachiopods. Note the extinction pattern of the brachiopod bioclast (B) mimicked by the overlying radiaxial and fascicular optic calcite cements. Crinoid bioclast is overlain by an early (I), inclusion-rich syntaxial cement (white arrow), and a later (II), clear syntaxial cement (black arrow) both in optical continuity with the crinoid bioclast. E and F. Microfacies 6. Partially silicified, grain-supported crinoid-brachiopod calcarenite with syntaxial calcite cement and baroque dolomite. Silica has replaced brachiopods, crinoids, and calcite cement. Late baroque dolomite (D) crosscuts and replaces the silicified brachiopod (center). The dark color of dolomite results from surface weathering which oxidized the iron of the dolomite. Photomicrograph F is the crossed nicols view of E. G. Microfacies 8. *Amphipora*-accumulated limestone with grain-supported intraclastic calcarenite matrix and abundant fabric-selective burial dissolution porosity (shades of gray areas). Burial dissolution dissolved cement, *Amphipora*, and calcisiltite matrix. Sample is impregnated with blue-dyed plastic. H. Microfacies 10. Grain-supported, intraclastic-pelletoidal calcarenite with calcisiltite matrix, fibrous cement, and scattered calcispheres. Stylolite is crosscut by late fracture filled with fibrous calcite cement demonstrating that fracturation occurred after stylolitization. All photomicrographs: plane polarized light, except D and F: crossed

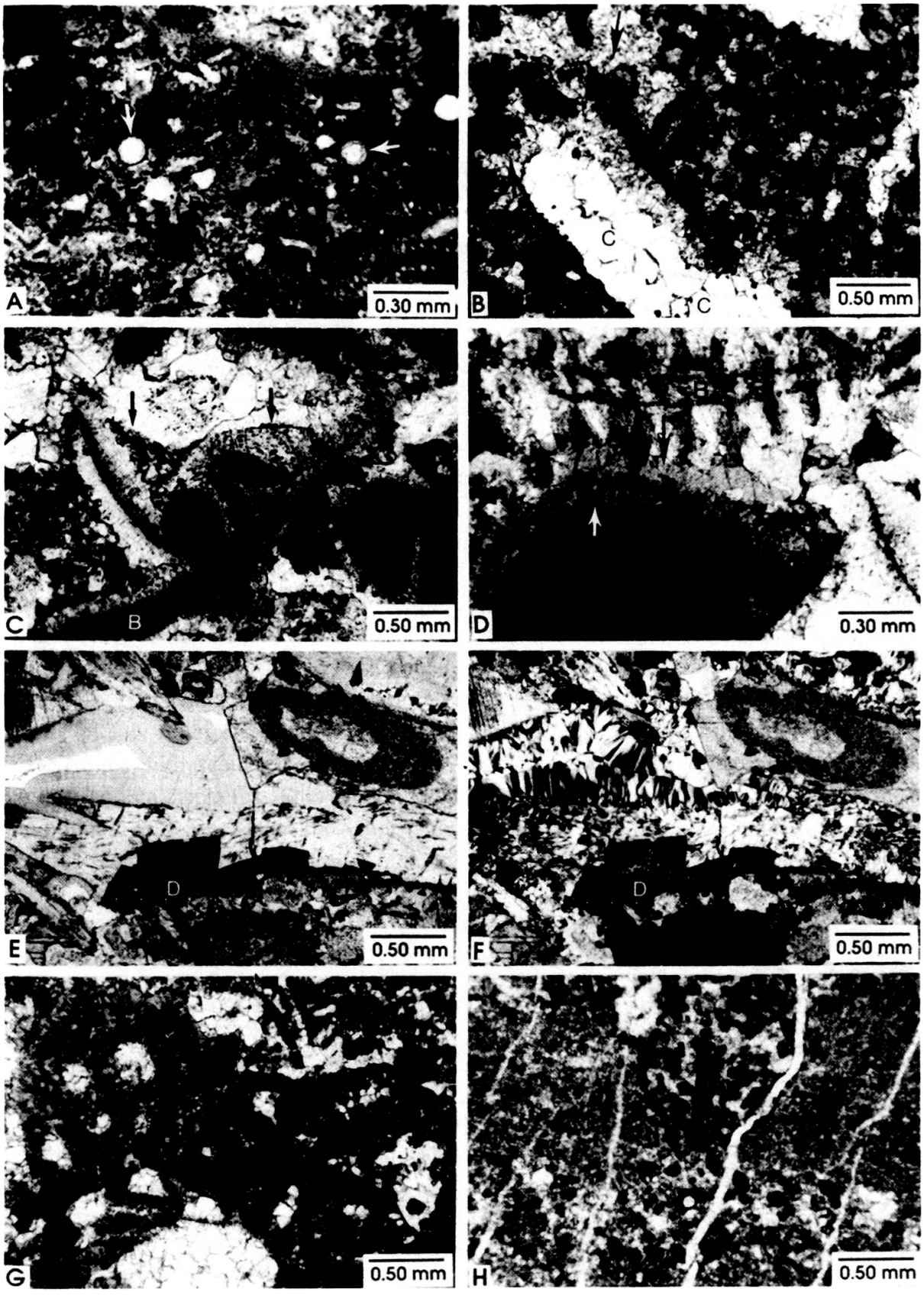
A
0.30 mm
B
C
C
0.50 mm
C
B
0.50 mm
D
0.30 mm
E
D
0.50 mm
F
D
0.50 mm
G
0.50 mm
H
0.50 mm

Marine Vadose

The diagenetic features attributed to this environment are the precipitation of gypsum and incipient dolomitization, both of which are very rare.

Meteoric Vadose

Features attributed to this environment are dissolution of gypsum, fabric and nonfabric selective dissolution (Plate 4, B), fracturation and vadose silt. Channels, vugs and molds produced by dissolution are commonly filled with vadose silt and/or calcite cement. Most of the products of the meteoric vadose environment are found in the intertidal flat environment (microfacies 11), with minor amounts in the *Amphipora*-accumulated limestone (microfacies 8).

Meteoric Phreatic Undersaturated

The products of this environment are fabric and nonfabric selective dissolution (Plate 4, B), dedolomitization (rhomb-shaped areas filled with microcrystalline calcite, similar to those in Plate 5, E) and fracturation. Most molluscan bioclasts were dissolved in this environment and latter filled with calcite cement.

Meteoric Phreatic Saturated

The dominant products of this environment were neomorphism, syntaxial cement (II) (Plate 4, D and E), bladed and equant calcite cements and microcrystalline calcite cement. Neomorphism is evident by the stabilization of early rim cements and the conversion of carbonate muds to pseudosparite and pseudomicrosparite. The most abundant cements are syntaxial cement (II) followed by bladed and equant calcite. These cements infill most of the primary porosity in the higher energy microfacies. Microcrystalline calcite cement occurs in small amounts and tends to be concentrated in fenestrae and small vugs where it typically overlies vadose silt. It is characterized by small equant calcite crystals that are generally less than 50 microns in size.

Mixed Marine-Meteoric

The diagenetic product of this environment (Knauth,1979) was silicification (II). It is minor and generally restricted to brachiopod and crinoid bioclasts with lesser amounts replacing cements and matrix (Plate 4, E and F). Silica occurs as microfibrous quartz, macroquartz and microquartz. Macroquartz is common in the calyxes of corals.

Burial

The products of this environment are dolomite (Plate 4, E and F), stylolites (Plate 4, H) and compaction (II), burial dissolution (Plate 4, H), fracturation and fracture-

FIG. 9.

Diagenetic evolution of normal marine microfacies.

DIAGENETIC FEATURE \ ENVIRONMENT		MARINE PHREATIC	MARINE VADOSE	METEORIC VADOSE	METEORIC PHREATIC UNDERSATURATED	METEORIC PHREATIC SATURATED	MIXED MARINE-METEORIC WATER	BURIAL
GLAUCONITE		▬						
PHOSPHATE		—						
PYRITE		▬						
NATIVE SULFUR		—						
MICRITE ENVELOPES AND MICRITIZATION		▬						
"BLUE-GREEN" ALGAL COATINGS		—						
BORINGS		—						
HARDGROUNDS		—						
EARLY LITHIFICATION		▬						
REWORKING OF INTRACLASTS		▬						
SILICIFICATION (I)		—						
COMPACTION (I)		—						
EARLY CEMENTS	RADIAXIAL CALCITE	—						
	FASCICULAR OPTIC CALCITE	—						
	SYNTAXIAL (I)	—						
	FIBROUS ISOPACHOUS	—						
PRECIPITATION OF GYPSUM			—					
INCIPIENT DOLOMITIZATION			—					
DISSOLUTION OF GYPSUM				—				
DISSOLUTION FEATURES				▬	—			
FRACTURATION				▬	—			
VADOSE SILT				▬				
DEDOLOMITIZATION					—			
NEOMORPHISM						—		
SYNTAXIAL CEMENT (II)						▬		
BLADED AND EQUANT CALCITE CEMENT						▬		
MICROCRYSTALLINE CALCITE CEMENT						—		
SILICIFICATION (II)							—	
BURIAL DOLOMITIZATION								▬
STYLOLITES AND COMPACTION (II)								▬
BURIAL DISSOLUTION								—
FRACTURATION AND FRACTURE-FILLING CALCITE								—

▬ COMMON
— RARE
— VERY RARE

TIME → TIME → TIME

filling calcite cement (Plate 4, H). The increased abundance of dolomite in beds next to shales, and rarity of extensive evaporitic flats and exposure features (which are common to other dolomite-forming models) suggest that most of the dolomite was formed in the burial environment and produced by precipitation and replacement from fluids released by the compaction of shales and illitization of smectite. These two processes may not have provided the large amount of magnesium needed to form the dolomite. Basinal fluids moving through the carbonates could have provided magnesium and dolomitized part of the sequence. Dolomite occurs mainly as nonferroan, unzoned, medium- to finely- crystalline rhombs which preferentially replaced the matrix. Ferroan dolomite is concentrated in beds that lie within a few meters of shales, suggesting the iron migrated out of the shales and into the carbonates.

Both sutured and nonsutured stylolites are common. All microfacies contain stylolites. Some stylolites appear to be associated with the development of a halo of secondary moldic porosity, but usually porosity near stylolitic zones is very low.

Burial dissolution occurred after compaction and cementation because both earlier cements and deformed bioclasts have been dissolved. Most of this secondary porosity is fabric selective, interparticle or intraparticle with rare nonfabric selective channels and vugs. Calcisiltite intraclasts, bryozoans and stromatoporoids appear to be selectively dissolved together with lesser amounts of calcite cement. Late fractures filled with fibrous calcite cement crosscut bioclasts, earlier cements and stylolites.

DIAGENESIS OF HYPERSALINE MICROFACIES

INTRODUCTION

The diagenesis of the hypersaline microfacies is dominated by dolomitization and formation of collapse breccias. As assumed in the hypersaline models, dolomite formed by either evaporative pumping, seepage refluxion or by a micro-dorag process. The hypersaline microfacies display diagenetic features indicating a general and usual evolution starting with marine phreatic and proceeding through marine vadose-evaporitic, meteoric vadose, meteoric phreatic, mixed marine-meteoric and ending with burial (Figure 10).

Marine Phreatic

The diagenetic products of this environment are dissolution features (half-moon ooids), early partial lithification, compaction, pyrite, and fibrous isopachous rim cements (Plate 5, A).

FIG. 10.

Diagenetic evolution of hypersaline microfacies.

DIAGENETIC FEATURE \ ENVIRONMENT	MARINE PHREATIC	MARINE VADOSE/ EVAPOR-ITIC	METEORIC VADOSE	METEORIC PHREATIC	MIXED MARINE/ METEORIC WATER	BURIAL
DISSOLUTION FEATURES (HALF-MOON OOIDS)	—					
EARLY PARTIAL LITHIFICATION	▬					
COMPACTION	—					
PYRITE	▬					
FIBROUS ISOPACHOUS RIM CEMENTS	—					
PRECIPITATION OF SALT, GYPSUM AND ANHDRITE		▬				
DOLOMITIZATION BY EVAPORATIVE PUMPING		▬				
DOLOMITIZATION BY SEEPAGE REFLUXION		▬				
VADOSE SILT			▬			
REPEATED EPISODES OF: 1. DISSOLUTION OF INTERBEDDED SALT			▬	—		
REPEATED EPISODES OF: 2. CALCITIZATION AND SILICIFICATION (I) OF GYPSUM AND ANHYDRITE			—	—		
REPEATED EPISODES OF: 3. FRACTURATION			▬	—		
REPEATED EPISODES OF: 4. COLLAPSE			▬	—		
FRACTURES FILLED WITH: 1. CARBONATE FLOW BRECCIA			▬			
FRACTURES FILLED WITH: 2. GYPSUM/ANHYDRITE			▬			
FRACTURES FILLED WITH: 3. VADOSE SILT			▬			
FRACTURES FILLED WITH: 4. SPARITE CEMENT				▬		
DEDOLOMITIZATION				—		
NEOMORPHISM				—		
MARGINAL REPLACEMENT OF SILICA BY CALCITE				—		
CALCITE CEMENT				▬		
FLUORITE					—	
DORAG DOLOMITIZATION					▬	
SILICIFICATION (II)					—	
NATIVE SULFUR					—	
COMPACTION (II)/STYLOLITES						▬
BURIAL DISSOLUTION						—
FRACTURATION AND FRAC-TURE-FILLING CALCITE						—

▬ COMMON
— RARE
— VERY RARE

→ TIME → TIME →

Half-moon ooids resulted from the dissolution of more soluble (evaporitic ?) concentric laminae (Carozzi, 1963). The dropped cores have more than one orientation suggesting reworking before final deposition.

Unusually thick, fibrous, isopachous rim cements occur on ostracods where their nucleation and growth was controlled by the fibro-radial structure of the ostracod test. They are usually 10 to 50 microns thick and can be dated as early, being truncated by dissolution related to the formation of collapse breccias and overlain by phreatic calcite cements and internal sediments.

Marine Vadose-Evaporitic

The precipitation of evaporites and dolomitization were the main features of this environment. Evidence of gypsum and anhydrite precipitation consists of length-slow chalcedony, calcitized chickenwire anhydrite, lath-shaped quartz crystals after anhydrite (Plate 3, E, arrows), megaquartz with gypsum crystal morphology (Plate 5, B), calcitized nodular gypsum (Plate 5, C), calcite pseudomorphs after clusters of gypsum crystals (Plate 5, D). Very minor amounts of anhydrite occur in megaquartz and lath-shaped quartz crystals as highly birefrigent inclusions with rectangular cleavage. The dolomite is very finely crystalline to aphanocrystalline, nonferroan and unzoned. Much of this dolomite occurs in intraclasts (microfacies H9).

Meteoric Vadose

The main diagenetic process associated with this environment is the formation of collapse breccias. This complex process produced both monomictic and oligomictic collapse breccias. The clasts are unsorted and angular, consisting of calcisiltites or

---

PLATE 5

Diagenesis of Hypersaline Microfacies

A. Microfacies H6. Ostracod-accumulated limestone with unusually thick, fibrous isopachous rim cements with polygonal interference boundaries (arrow). B. Silicified gypsum. Quartz has interlocking texture and morphology similar to intergrown gypsum crystals, demonstrating replacement of gypsum by silica. C. Calcitized nodular gypsum in dolomite matrix. Calcite retains the nodular morphology and curved concentric crystal faces (arrow) characteristic of gypsum. D. Microfacies H1. Calcite pseudomorphs after clusters of gypsum crystals. Gypsum crystals grew in carbonate mud, dissolved and molds were infilled with geopetal internal sediment and microsparite cement. E. Microfacies H7. Slightly laminated pelletoidal, pyritic, organic-rich calcisiltite with dedolomitization texture. Rhombic shapes are filled with microsparite and interpreted as dissolved dolomite rhombs infilled with microsparite. F. Microfacies H9. Partially dolomitized collapse breccia showing clast (D), dolomitized matrix (bottom), and calcite cement. Cubic-shaped fluorite crystal (arrow) shows partially dissolved core. Silicified anhydrite (A) occurs in dolomitized matrix. G. Monomictic calcisiltite collapse breccia. Clasts consist of pyritic unfossiliferous calcisiltite, set in a different lighter-colored interstitial calcisiltite matrix and microsparite cement. Typical puzzle-like texture indicates small displacement. H. Oligomictic calcisiltite collapse breccia. Clasts are several types of bituminous (large clasts at center) and nonbituminous unfossiliferous calcisiltites. Interstitial material consists of smaller calcisiltite clasts, calcisiltite matrix, and sparite cement. All photomicrographs: plane polarized light, except B: crossed nicols.

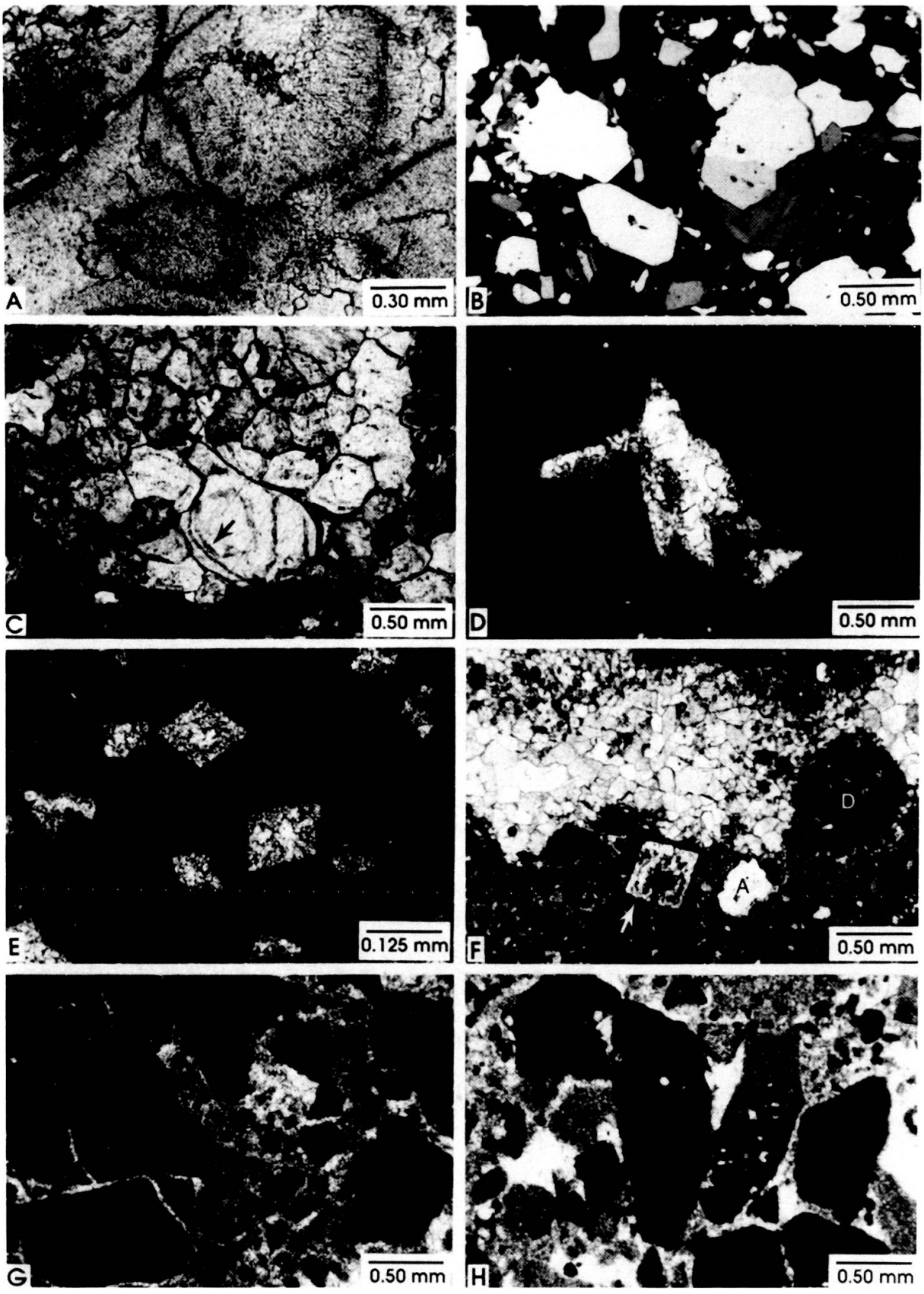
A
0.30 mm
B
0.50 mm
C
0.50 mm
D
0.50 mm
E
0.125 mm
F
D
A
0.50 mm
G
0.50 mm
H
0.50 mm

dolomitized calcisiltites representative of hypersaline microfacies. The fractures are filled with carbonate flow breccia (grain-supported, angular calcisiltite breccia with a calcisiltite matrix), calcisiltite, calcite cement, or vadose silt. Gypsum and anhydrite pseudomorphs are locally abundant in the matrix.

These breccias formed by the dissolution of interbedded halite, which resulted in the fracturation and collapse of the overlying beds. This process accounts for the angularity of the clasts, puzzle-like texture in the monomictic breccias, composition of the clasts and matrix, restriction of the breccias to the hypersaline microfacies, and abundance of the breccias in the supratidal microfacies (H9). The presence of calcisiltite, which flowed between the clasts, suggests that dissolution and collapse started prior to complete lithification. More than one phase of dissolution and collapse is demonstrated by the fracturation of earlier lithified collapse breccias, forming clasts within clasts.

Meteoric Phreatic

The process of dissolution of halite and collapse that started in the meteoric vadose environment probably continued into this environment as suggested by the presence of sparite cement in fractures cutting collapse breccias. Other processes were dedolomitization (Plate 5, E), neomorphism, marginal replacement of silica by calcite, calcite cementation (Plate 5, G and H), and fluorite precipitation (Plate 5, F).

Dedolomitization occurs as rhombic shapes filled microsparite and as iron-stained calcite rhombs that resemble zoned dolomite rhombs. The transformation of unstable carbonates to stable calcite is best illustrated by the complete neomorphism of some ooids to pseudosparite. Fractures, fenestrae, and primary porosity are commonly filled with microsparite or sparite cement. These cements typically overlie vadose silt and carbonate flow breccias.

At Fayette Quarry (outcrop FQ in Figure 2) the top several meters of the Wapsipinicon Formation contain scattered euhedral crystals of clear fluorite. The fluorite may be partially dissolved, possibly due to surface weathering, and occurs only in matrix of the collapse breccias. Restriction of the fluorite to the matrix in the top few meters of the Wapsipinicon, lack of other hydrothermal minerals, and report of sedimentary barite nearby (Pearson, 1982) suggest a diagenetic origin. Fayette Quarry is at the extreme edge of the Upper Mississippi Valley Lead-Zinc district, and a hydrothermal origin for the fluorite cannot be completely ruled out. Moore and others (1972) reported diagenetic fluorite in a carbonate sequence and concluded that fluorine was concentrated in the aragonitic muds and released during early dolomitization. The same process could account for the fluorite at Fayette Quarry.

Mixed Marine-Meteoric

The processes occurring in this environment were dolomitization, silicification and precipitation of native sulfur. Dolomite occurs as medium crystalline, nonferroan, unzoned rhombs scattered in the calcisiltite matrix. Native sulfur is rare and found only

in beds containing calcite pseudomorphs after gypsum or anhydrite. Native sulfur probably resulted from the partial oxidation of hydrogen sulfide produced by sulfate-reducing bacterial action on sulfate minerals.

Burial

Many of the same processes and products of the burial diagenetic environment of the normal marine sequence are also represented in the hypersaline microfacies. Compaction, dolomitization, stylolites, burial dissolution, fracturation, and fracture-filling calcite appear similar and are not further discussed. However early dolomites may have been altered by the fluids related to burial dolomitization.

STRATIGRAPHIC SECTIONS AND VERTICAL SUCCESSION OF MICROFACIES

The petrographic data derived from the study of the thin sections were plotted for all stratigraphic sections (Kocken,1989). These representations consist from left to right of:

1) Column with microfacies symbols (key in Figure 4), control points and core depth or height above base of outcrop in meters.

2) Curves representing clasticity and frequency of major components, percent matrix, cement, stromatolites and dolomite, and dolomite crystal size.

3) Simplified sketches of the depositional models, in the lower right of the diagrams, were used as scales for environmental interpretation. Model 3 is plotted to the left of Model 4 to portray their normal evolution through time. Changes between hypersaline and normal marine models are shown by a horizontal line in the environmental interpretation curve with the corresponding models labeled above and below. Cycle boundaries are shown by vertical arrows with related numbers.

Among the numerous shallowing-upward sequences of the four models (Kocken, 1989), only two typical examples are given here: for normal marine conditions of model 1 at section TQ (Figure 11) and for hypersaline conditions of models 3 and 4 at section CQ (Figure 12).

CYCLICITY, CORRELATION OF CYCLES IN THE MIDDLE DEVONIAN AND BASINWIDE IMPLICATIONS

CYCLICITY IN THE MIDDLE DEVONIAN

Shallowing-upward cycles are fundamental features of carbonate rocks (Carozzi, 1989). These cycles reflect that carbonate production and accumulation are usually greater than the combined effect of tectonic subsidence and eustatic sea level rise.

Consequently, carbonate sediments rapidly accrete toward sea level producing shallowing-upward cycles. These cycles are commonly associated together in larger sequences that also show a shallowing-upward trend.

The combination of local subsidence and global eustatic sea level rise in the Middle Devonian in the central midcontinent led to the superposition of shallowing-upward cycles. Each cycle reached its peak in successively deeper water, forming a larger sequence with a deepening-upward trend. This evolution, which terminated in basinal shales, indicates that the combined effect of local subsidence and global eustatic sea level rise overcame a series of unsuccessful accreting attempts by carbonate production and accumulation.

The most typical example is documented by outcrops of sections GT1 and GT 2 (Figure 13). The deepening-upward sequence consists of four shallowing-upward cycles (labeled 1 to 4) with each cycle reaching its peak in successively deeper water.

CORRELATION OF CYCLES IN THE MIDDLE DEVONIAN

Thirteen shallowing-upward cycles were recognized from the stratigraphic sections. Contacts between the cycles were placed at the point of maximum shallowing because it is believed these events represent traceable basinwide phenomena. Cycles were correlated using stratigraphic position, cycle shape and thickness and relative magnitude of the deepening phase. The cyclicity and cycle correlations are summarized in three cross sections (Figures 13, 14 and 15). Individual shallowing-upward cycles can be correlated from one location to the next if the distance between them is less than about 75 kilometers, provided they are in a similar depositional setting. With greater distances, only the larger cycles can be correlated.

The first five cycles are best developed in the Grand Tower Limestone and Lingle Formation (Figure 13). Cycle 1 represents the initial transgression of Middle Devonian in Illinois and contains only shallow water microfacies. Cycle 2 shows a typical shallowing-upward character, however the deepening phase above it at the base of cycle 3 is poorly developed in GT1 and GT 2. The deepening associated with cycle 4 is very pronounced. At the Tuscola quarry, shallow water hypersaline microfacies grade to normal marine basinal microfacies, in GT1 and GT 2, the base of this cycle marks the first occurrence of the deepest water microfacies. This cycle correlates with the onset of deposition of the Wapsipinicon Formation north of the Sangamon Arch (Figures 14 and 15). However, sea level rise associated with this cycle was not large enough to flood the Sangamon Arch as hypersaline conditions prevailed north of the Arch and normal marine conditions south of it. Overall, cycles 1 through 4 show a pronounced deepening

---

FIG. 11.

Model 1. Example of component variations at Tuscola quarry (29.8 to 36.0 m).

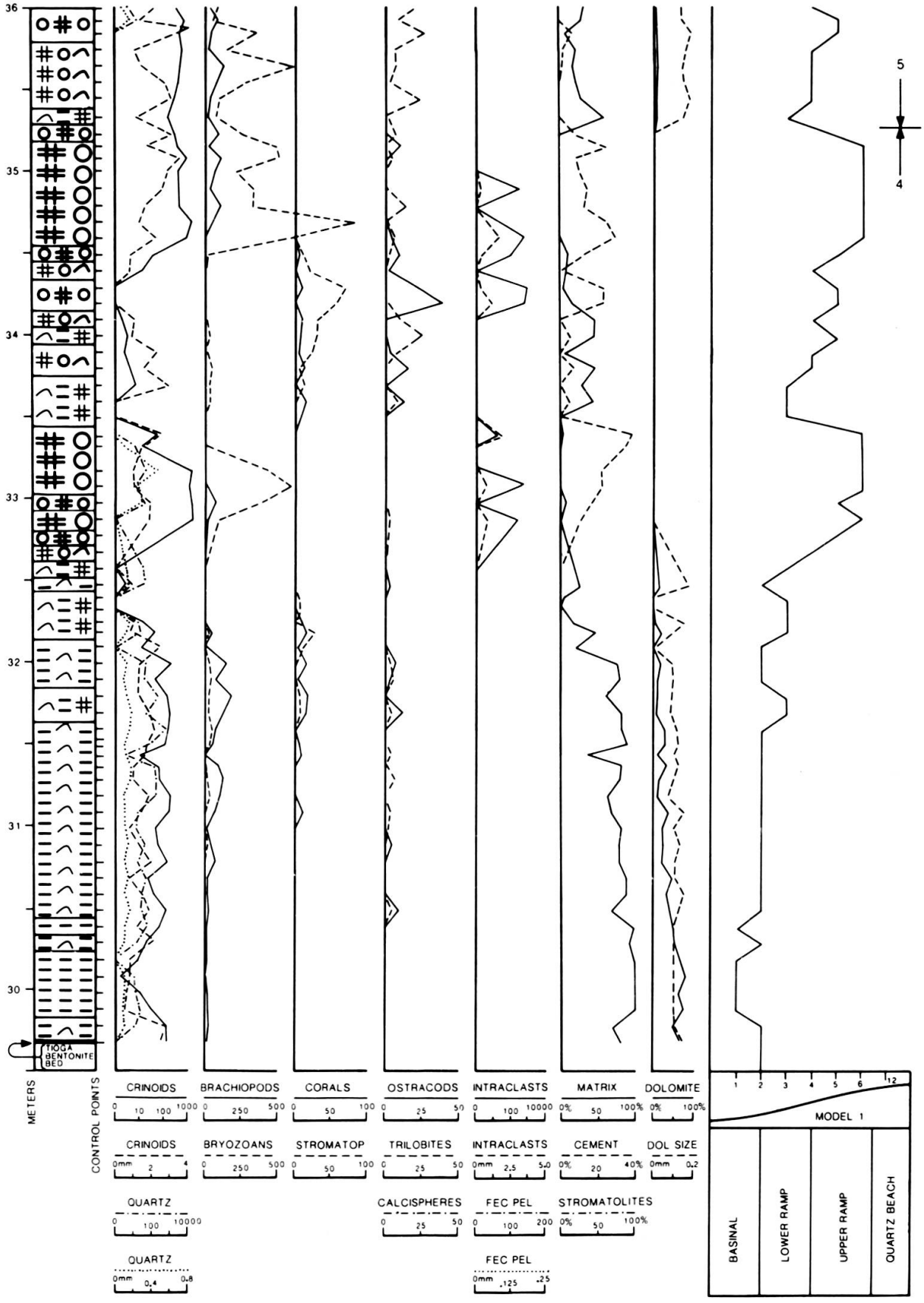
36
35
34
33
32
31
30
METERS
TIOGA BENTONITE BED
CONTROL POINTS
CRINOIDS
BRACHIOPODS
CORALS
OSTRACODS
INTRACLASTS
MATRIX
DOLOMITE
CRINOIDS
BRYOZOANS
STROMATOP
TRILOBITES
INTRACLASTS
CEMENT
DOL SIZE
QUARTZ
CALCISPHERES
FEC PEL
STROMATOLITES
QUARTZ
FEC PEL
5
4
MODEL 1
BASINAL
LOWER RAMP
UPPER RAMP
QUARTZ BEACH

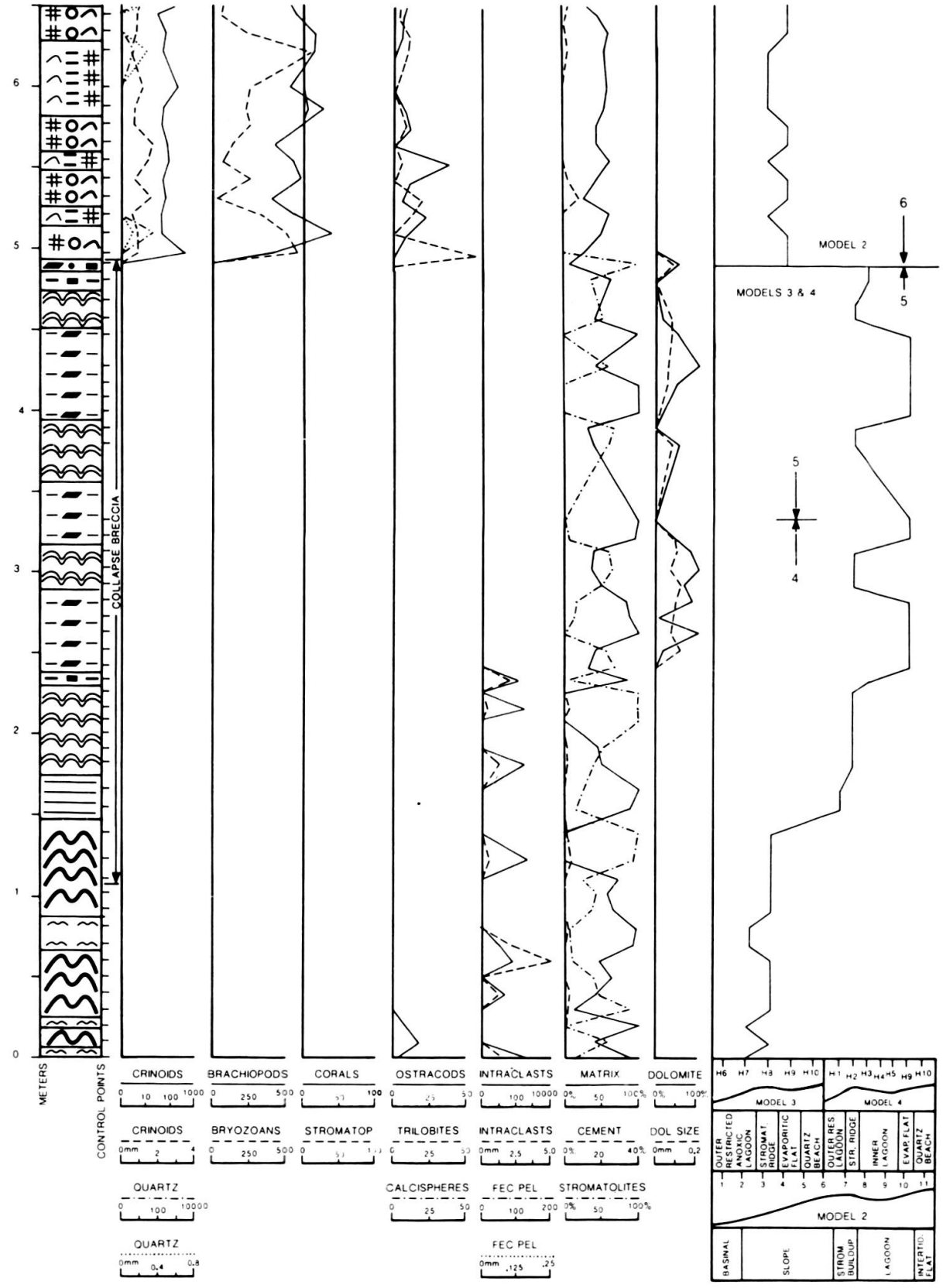

FIG. 12.

Models 3 and 4. Example of component variations at Conklin quarry (0 to 6.5 m).

trend that started with shallow water microfacies in cycle 1 and ended with deep water microfacies in cycle 4.

Correlation of cycles 4, 5 and 6 between sections south and north of the Sangamon Arch (Figures 13, 14 and 15) is complicated by the lack of available late Middle Devonian age sections in Southern Illinois, the presence of an erosional disconformity between the Wapsipinicon Formation and Cedar Valley Limestone, and by extensive collapse breccias in the Wapsipinicon Formation which make recognition of cycles less reliable.

Cycle 5 is truncated north of the Sangamon Arch (Figures 14 and 15) by the disconformity at the top of the Wapsipinicon Formation. Cycles 6 through 13 (Figures 14 and 15) are well developed north of the Sangamon Arch because these sections are late Middle Devonian in age compared to the early Middle Devonian age for the sections south of the Arch. The transgressive sequence at the base of cycle 6 corresponds to the rise in eustatic sea level associated with the Taghonic Onlap and onset of deposition of the Cedar Valley Limestone.

Cycles 7 and 8 (Figures 14 and 15) are small cycles with several poorly developed smaller shallowing phases within them. Cycle 9 generally represents a shallowing from basinal or lower slope microfacies to lagoonal or intertidal microfacies and is followed by cycle 10 which is characterized by thick accumulation of lagoonal and intertidal microfacies in cores D9 and D6. Cycles 11 and 12 are small cycles that do not contain deeper water microfacies and are best preserved in sequences close to the Ozark Dome (Figure 15). Cycle 13 represents a large deepening event where the intertidal and

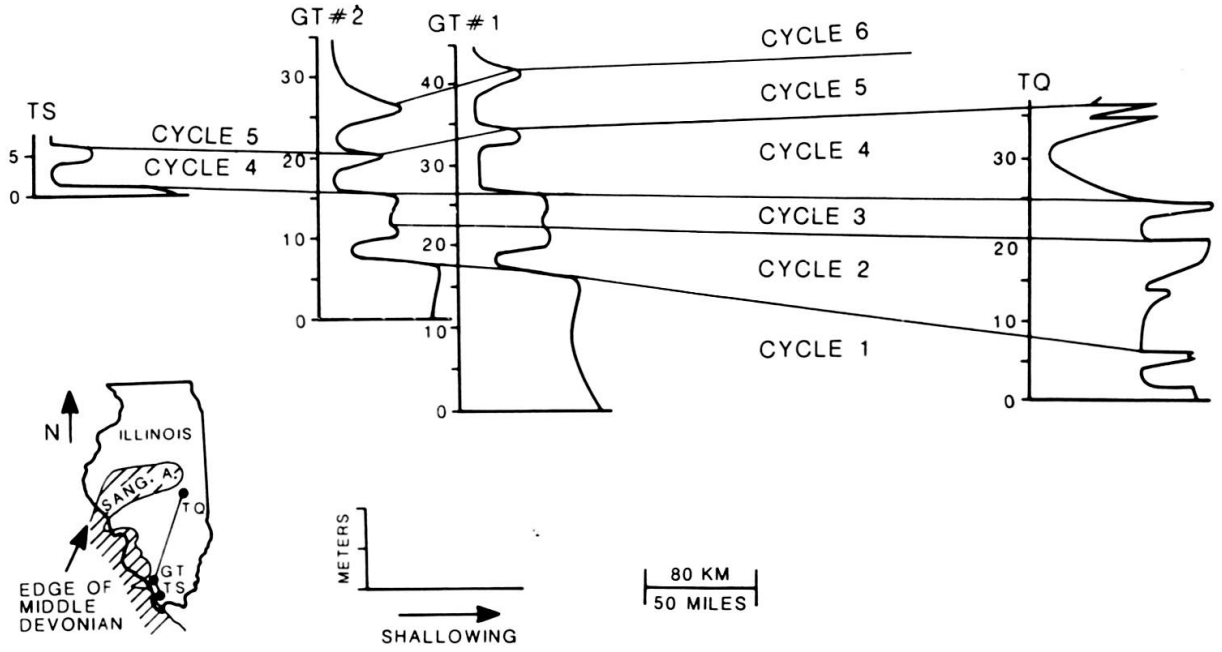

FIG. 13.

Correlation of cycles along cross section from Tuscola quarry to Trip School section, Grand Tower Limestone and Lingle Formation.

lagoonal microfacies of cycle 12 are overlain by lower slope or basinal microfacies. This deepening corresponds to the onset of Upper Devonian shale deposition.

COMPARISON OF CYCLES IN THE GRAND TOWER LIMESTONE NEAR THE SANGAMON ARCH WITH THOSE OF THE WITTENBERG TROUGH

The cycles in the normal marine portion of the Grand Tower Limestone near the Sangamon Arch (cycle 4 at Tuscola quarry in Figure 13) are thinner, may contain more than one shallowing phase, and are more asymmetrical compared to the corresponding cycles in the Wittenberg Trough (Sections GT1 and GT 2 in Figure 13). These differences probably reflect that the Wittenberg Trough was undergoing active subsidence while the Sangamon Arch was stable. Hence carbonates deposited close to the Sangamon Arch display cycle shape and thickness characteristic of most carbonates while cycles in the subsiding Wittenberg Trough are thicker and more symmetrical.

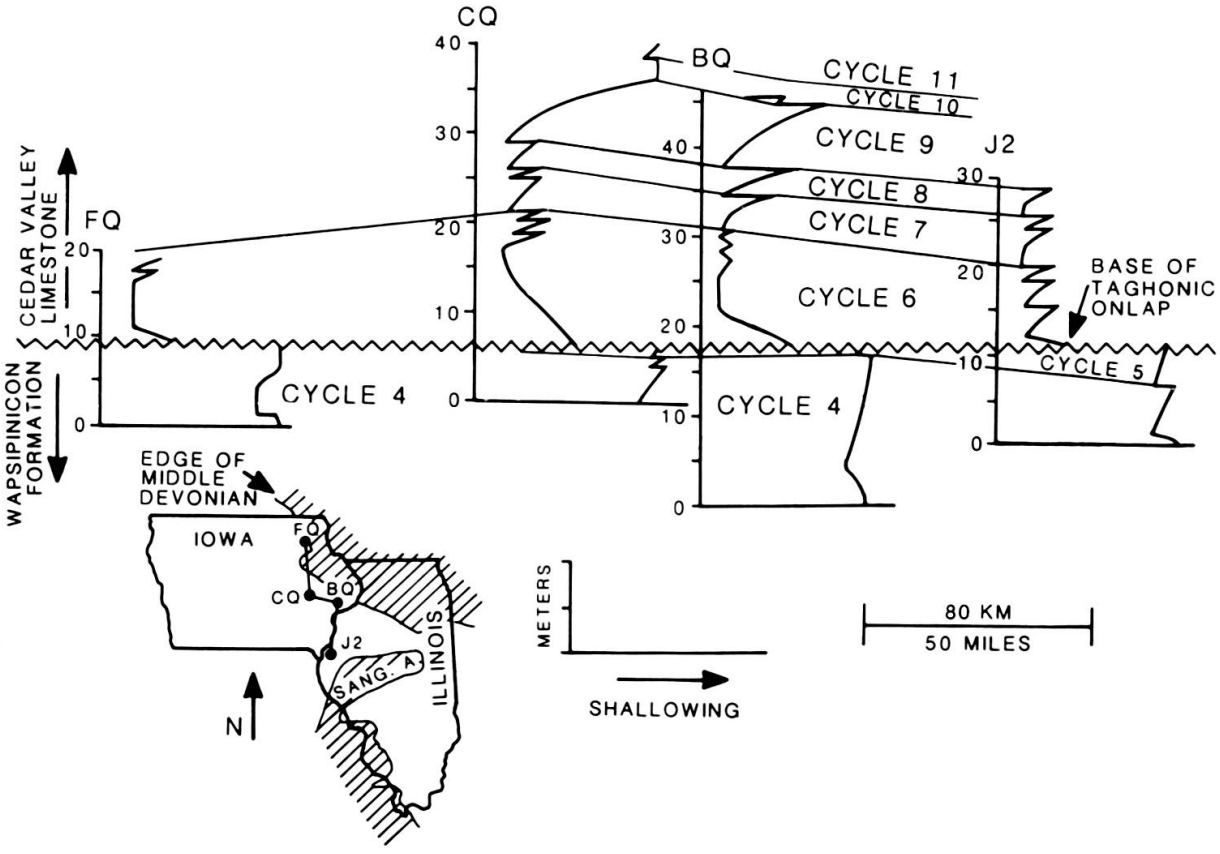

FIG. 14.

Correlation of cycles along cross section from Fayette quarry to Core J2.

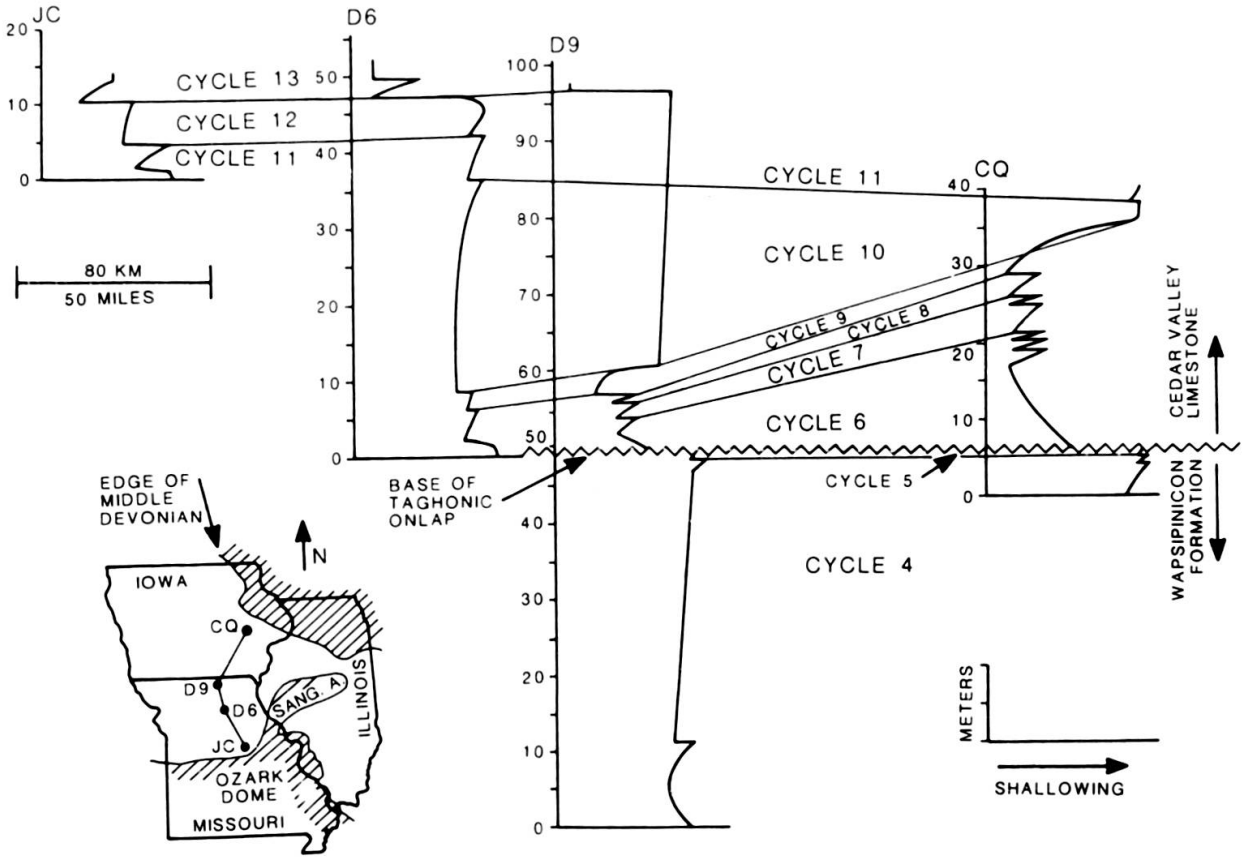

FIG. 15.

Correlation of cycles from Conklin quarry to Jefferson City outcrops.

CORRELATION OF CYCLES WITH EUSTATIC SEA LEVEL CURVES

The 13 shallowing-upward cycles illustrated in the cross sections (Figures 13, 14, and 15)) were correlated (Figure 16) using published conodont zones and stratigraphic relationships with the cycles recognized by Johnson and others (1985). Cycles 1 though 4 correlate very well with their cycles Ic to Ie. At Tuscola quarry, cycle 2 contains two shallowing events which correlate with the sea level oscillations at the top of Ic and the base of Id. Cycle 5 does not contain the numerous oscillations seen in If; this reflects the problems correlating between cycles 5 and 6 as discussed above. Cycles 6 through 13 directly correlate with the sea level oscillations documented by Johnson and others (1985) if cycle 7 and 8 are considered as one cycle. However the presence of numerous small shallowing-upward cycles in 6, 7 and 8 suggest that there may be more small oscillations in cycle IIa, or carbonate production was periodically greater than the combined effects of sea level rise and subsidence. The correlation of cycle 13 with IIc shows that the uppermost part of the Cedar Valley Limestone is earliest Late Devonian in age.

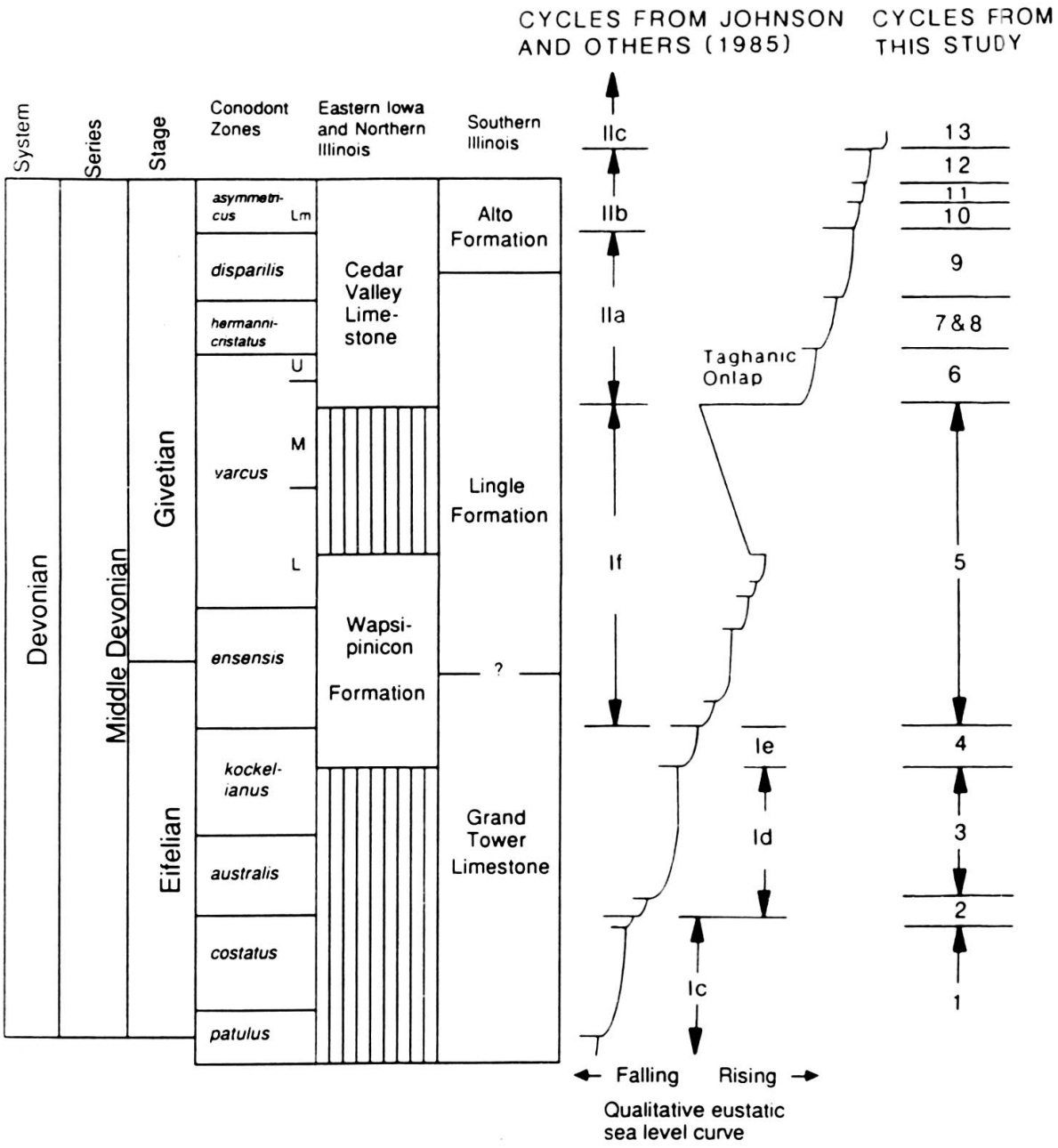

FIG. 16.

Comparison of cycles from the Wapsipinicon Formation, Cedar Valley Limestone, Grand Tower Limestone, and Lingle Formation with cycles after Johnson and others (1985).

Taken as a whole the Middle Devonian was a time of rising sea level with many oscillations. For example this rise is demonstrated by the deepening-upward sequence at sections GT1 and GT 2. In other sections, normal marine rocks overlie hypersaline rocks both north and south of the Sangamon Arch indicating a general deepening of the environment, although complicated by small-scale shallowing-upward cycles and episodes of stability. Final deepening is shown by Upper Devonian shales overlying the

carbonate sequence. The overall pattern of rising sea level is interrupted by an episode of sea level fall associated with the disconformity between the Wapsipinicon Formation and Cedar Valley Limestone.

Possible origins for the Middle Devonian cycles has been reviewed by Johnson and others (1985). They concluded the cycles may have resulted from episodes of mid-plate thermal uplift and submarine volcanism. The lack of evidence for continental glaciation during the Middle Devonian rules out glacial retreats and advances as a possible mechanism. The Middle Devonian sequences used in this study contain only an incomplete recording of the cyclicity reflecting its cratonic setting (separate depocenters and local control on deposition), abundance of hypersaline deposits, and small disconformities. These problems make it difficult to postulate an origin for the cycles seen in the Middle Devonian.

CONCLUSIONS

The Middle Devonian sequences in eastern Iowa, Missouri, and Illinois can be divided into 24 microfacies, 12 deposited in a hypersaline environment and 12 in normal marine. From the stratigraphic sections and statistical relationships between microfacies four ideal shallowing-upwards sequence were developed which were interpreted as depositional models according to Walther's Law. Models 1 and 2 represent normal marine conditions and Models 3 and 4 hypersaline conditions.

Model 1 expresses the normal marine sequences south of the Sangamon Arch, corresponding to the Grand Tower Limestone and Lingle Formation. It is a carbonate ramp with a quartz sand beach and terminates in a basinal environment.

Model 2 represents the normal marine, Cedar Valley Limestone which occurs north of the Sangamon Arch and is slightly younger than the Grand Tower Limestone. This model is a carbonate platform with a frontal buildup and consists in an offshore direction of five environments: intertidal flat, ecologically zoned lagoon, stromatoporoid buildup, slope and basinal. The slope and basinal microfacies are the same as the ramp and basinal microfacies in Model 1.

The twelve hypersaline microfacies define Model 3 and 4 which follow each other in vertical sequence. Model 3 represents the Kenwood and Spring Grove member of the Wapsipinicon Formation. It is a partly anoxic hypersaline environment consisting, in a offshore direction, of a quartz sand beach, evaporitic flat, stromatolitic ridge, and an anoxic lagoon. This model is characterized by bituminous microfacies in the anoxic lagoon and a stromatolitic ridge.

Model 4 is applicable to the Wapsipinicon Formation, Geneva Dolomite, and parts of the Cedar Valley Limestone and hence represents the typical Middle Devonian hypersaline environment. This model displays in a offshore direction a quartz sand beach, evaporitic flat, inner lagoon, stromatolitic ridge, and outer lagoon. The quartz sand beach and evaporitic flat are similar to those in Model 3.

Two diagenetic sequences were recognized, one for the normal marine microfacies and the other for the hypersaline microfacies. Normal marine microfacies display diagenetic features indicating a general evolution starting with marine phreatic and proceeding through marine vadose, meteoric vadose, undersaturated meteoric phreatic, saturated meteoric phreatic, mixed marine-meteoric, and ending with burial.

Diagenesis of the hypersaline microfacies was dominated by dolomitization and formation of collapse breccias. The dolomite formed early by either evaporitic pumping, seepage refluxion, or by a micro- dorag process. Collapse breccias are restricted to the Wapsipinicon Formation and formed by dissolution of interbedded halite. The hypersaline microfacies display diagenetic features indicating a general normal progression starting with marine phreatic and proceeding through marine vadose-evaporitic, meteoric vadose, meteoric phreatic, mixed marine-meteoric, and burial.

The Middle Devonian sections are dominated by shallowing-upward cycles which reach their peaks in successively deeper water forming larger sequences with a deepening-upward trend. These conditions result from the fact that local subsidence and global eustatic sea level rise overcame a series of unsuccessful accretionary attempts by carbonate production and accumulation. The Grand Tower Limestone in the Wittenberg Trough contains a spectacular deepening-upward sequence composed of four shallowing-upward cycles with each cycle reaching its peak in increasingly deeper water, a situation resulting from active subsidence.

Thirteen shallowing-upward cycles were recognized from the stratigraphic sections. The first four cycles are well developed in the Grand Tower Limestone and express an overall deepening evolution. Cycle 4 has a very pronounced deepening at its base which correlates with the onset of deposition of the Wapsipinicon Formation north of the Sangamon Arch. Correlation between section north and south of the Sangamon Arch is difficult because of the lack of late Middle Devonian age sections in southern Illinois, the presence of collapse breccias in the Wapsipinicon and by the disconformity at the top of the Wapsipinicon. Cycles 6 through 13 are well developed in the Cedar Valley Limestone north of the Sangamon Arch. These cycles appear to correlate well with published Middle Devonian sea level curves and confirm that the Middle Devonian was a time of oscillating sea level rise.

ACKNOWLEDGEMENTS

We thank S. P. Altaner, T. F. Anderson, D. B. Blake, and R. L. Langenheim Jr for their constructive criticisms of this paper which is a portion of the doctoral dissertation of R. J.K. completed under the supervision of A.V.C.

We are very grateful for the financial support made available for this investigation by a grant from TEXACO USA to A.V.C. and from the Department of Geology at the University of Illinois. The State Geological Surveys of Missouri and Illinois are thanked for generously providing core samples.

REFERENCES

BUNKER, B. J., WITZKE, B. J., WATNEY, W. L., and G. A. LUDVIGSON (1988). Phanerozoic history of the central midcontinent, United States: In L. L. SLOSS (Editor), *The geology of North America*. U.S. Geol. Surv., Boulder, Colorado, D-2, pp. 243-260.

CAROZZI, A. V. (1963). Half-moon oolites: *Jour. Sed. Petrology*, v. 33, pp. 633-645.

— (1989). *Carbonate rock depositional models, a microfacies approach.* Advanced Reference Series. Prentice Hall, Englewood Cliffs, New Jersey, 604 p.

CAROZZI, A. V. and M. S. GERBER (1978). Synsedimentary chert breccia: A Mississippian tempestite: *Jour. Sed. Petrology*, v. 48: pp. 705-708.

COLLINSON, C., BECKER, L. E., JAMES, G. W., KŒNIG, J. W., and D. H. SWANN (1967). Devonian of the north-central region, United States: In D. H. OSWALD (Editor), *International symposium on the Devonian System*. Alberta Soc. Petroleum Geologists, Calgary, Canada, v.1, pp. 933-971.

COLLINSON, C. (1988). Illinois Basin Region: *In* L. L. SLOSS (Editor), *The geology of North America*. United States Geol. Surv., Boulder, Colorado, D-2: pp. 383-426.

JOHNSON J. G., KLAPPER, G., and C. A. SANDBERG (1985). Devonian eustatic fluctuations in Euramerica: *Geol. Soc. America Bull.*, v.96, pp. 567-587.

KALDI, J. and J. GIDMAN (1982). Early diagenetic dolomite cements: Examples from the Permian Lower Magnesian Limestone of England and the Pleistocene carbonates of the Bahamas: *Jour. Sed. Petrology*, v. 52, pp. 1073-1085.

KNAUTH, L. P. (1979). A model for the origin of chert in limestone: *Geology*, v.7, pp. 274-277.

KOCKEN, R. J. (1989). Carbonate microfacies, depositional models, and diagenesis of the Middle Devonian in Illinois, Eastern Iowa, and Missouri: *Unpubl. Ph. D. thesis, Univ. Illinois (Urbana-Champaign)*, 160 p.

MEENTS, W. F. and D. H. SWANN (1965). Grand Tower Limestone (Devonian) of southern Illinois: *Illinois State Geol. Survey Circular* 389, 33 p.

MIDDLETON, G. V. (1973). Johannes Walther's Law of the correlation of facies: *Geol. Soc. of America Bull.*, v. 84, pp. 979-988.

MOORE, C. A. Jr., SMITHERMAN, J. M., and S. H. ALLEN (1972). Pore system evolution in a Cretaceous carbonate beach sequence: *24th International Geological Congress*, Montreal, v. 6, pp. 124-136.

PEARSON, S. G. (1982). Depositional environments, diagenesis, and barite mineralization of the Middle Devonian Wapsipinicon Formation in Fayette County, Iowa: *Unpubl. M.S. thesis, Univ. of Iowa, Iowa City, Iowa*, 203 p.

SAS INSTITUTE INC. (1987 a). *SAS user's guide. Basics version*: SAS Institute, Cary, North Carolina, 5th edition, 1290 p.

— (1987 b). *SAS user's guide. Statistics version*: SAS Institute, Cary, North Carolina, 5th edition, 956 p.